To the Graduate Council:

I am submitting herewith a thesis written by Darryl B. Glanton entitled "Correlating Grain Boundary Microstructure and Ductility Loss on Aging in Haynes® 25." I have examined the final electronic copy of this thesis for form and content and recommend that it be accepted in partial fulfillment of the requirements for the degree of Master of Science, with a major in Materials Science and Engineering.

___Easo P. George, Major Professor___

We have read this thesis
and recommend its acceptance:

___Claudia J. Rawn_____

___James R. Morris_____

Accepted for the Council:

_____

Carolyn R. Hodges, Vice Provost and
Dean of the Graduate School

(Original signatures are on file with official student records.)

Correlating Grain Boundary Microstructure and Ductility Loss on Aging in Haynes® 25

A Thesis

Presented for the

Master of Science

Degree

The University of Tennessee, Knoxville

Darryl Britt Glanton

December 2007

DEDICATION

This thesis is dedicated to my father, the late Robert A. Glanton for always believing in me and encouraging me to give my best in all of my life endeavors.

Acknowledgments

would like to thank all those who played a part in my completion of my Master of Science degree. I would like to thank Dr. Easo George for his guidance and mentorship in conducting my research. I would like to thank Bob Swindeman, John Shingledecker, and Dr. Edgar Lara-Curzio for introducing me to high temperature alloys and for always being willing to share their knowledge and experience with me. I would like to thank Dr. Yukinori Yammamoto and Neal Evans for introducing me to electron microscopy and for their time and patience in assisting me with my analysis. I would also like to thank Dr. James Morris and Dr. Claudia Rawn for serving on my committee.

Lastly, I would like to thank my family and friends, whose support and encouragement made this work possible.

This work was supported by the U.S. Department of Energy under Contract DE-AC05-00OR22725 with UT-Battelle, LLC, and through the Oak Ridge Institute of Science and Education (ORISE) post-bachelor's research program managed by Oak Ridge Associated Universities (ORAU).

Abstract

Haynes® 25 is a cobalt-base superalloy known for its excellent high temperature strength and corrosion resistance. However, this alloy undergoes severe embrittlement on aging at elevated temperatures. Historical research associated this ductility loss with the formation of a Co_2W Laves phase, but more recent studies have challenged the existence of this phase after prolonged aging at temperatures above 600°C. In this study, scanning and transmission electron microscopy were used to characterize the chemistry and location of precipitates in the alloy after aging at temperatures of 675 and 850°C for times up to 12,000 hours. These data were compared with tensile data from the same heat of material in an attempt to develop quantitative relationships between microstructural observations and ductility loss. It was found that the change in fractional coverage of the grain boundaries by a M_6C carbide precipitate (composition $W_3Co_{1.5}Cr_{1.5}C$) on aging correlates well with ductility loss on aging at 850°C. The change in fractional coverage on aging at 675°C did not correlate as well, suggesting that the prevalent mechanism for ductility loss at this temperature may not be the precipitation reaction.

Table of Contents

List of Tables

List of Figures

Introduction

Haynes® 25, also referred to as L-605, is a solid solution cobalt-base superalloy noted for its good formability, weldability, wear resistance, and strength at elevated temperatures. Its uses include gas turbines, nuclear reactor components, and surgical implants.[1,2] The nominal composition of Haynes® 25 is shown below in Table 1 while the composition used in this study is shown in Table 2.

It has been well-documented that Haynes® 25 experiences a severe loss in ductility after aging over the temperature range of about 600°C to 900°C, and early research suggested that a precipitation reaction resulting in Laves-Co_2W on the grain boundaries was the main cause of embrittlement.[3,4,5] However, one recent study suggests that, while Haynes® 25 does indeed suffer from a loss in ductility, the Laves phase is not the culprit and may not even exist in the material after aging at 550-1000°C .[6]

Table 1: Nominal Composition of Haynes® 25, weight percent[1]

Co[a]	Ni	Cr	W	Fe*	Mn	Si*	C
51	10	20	14	3	1.5	0.4	0.1
[a]as balance *maximum							

Table 2: Composition of Haynes® 25 used in this study, weight percent

Co[a]	Ni	Cr	W	Fe*	Mn	Si*	C
Bal.	10.32	20.23	14.77	2.34	1.51	0.16	0.11
[a]as balance *maximum							

Literature Review

Stanislaw Wlodek was among the first scientists to study the effects of aging on the ductility of Haynes® 25.[3] In his research, Wlodek performed bend tests on nine different heats of material after various aging conditions. He found that aging in the temperature range from 650°C to about 1100°C produced brittle intergranular fracture. With the aid of x-ray and electron diffraction, Wlodek identified two cubic metal carbide phases of type M_6C and $M_{23}C_6$ with respective chemical formulae of Co_3W_3C and $Cr_{23}C_6$, trace amounts of cubic zirconium carbonitride inclusions, and a hexagonal Laves phase with the probable chemical formula of $(Co,Ni)_2(Cr,W)$. For the sake of simplicity, this Laves phase has traditionally been assigned the nominal chemical formula of Co_2W. A summary of Wlodek's findings are shown in Table 3.

In his research, Wlodek attributed the loss in ductility to the formation of the Laves-Co_2W phase on and near the grain boundaries. He also noted that while cobalt and tungsten satisfy the radius criterion for the formation of A_2B Laves phase, their electron concentration ratios slightly exceed the maximum. Wlodek suggested that Si, an element known to reduce electron concentration in the Co-Cr-W ternary system, may be responsible for stabilizing the Laves phase. He speculated that the alloy compositions least susceptible to embrittlement would have silicon contents below 0.5 weight percent and iron contents of about two to three weight percent.

Despite his assertions, Wlodek acknowledged the low likelihood of silicon serving as a Laves phase stablizer since it is a trace impurity in the alloy. He points to statistical reasons which would make such a process very thermodynamically difficult.

Table 3. Phases reported by Wlodek[3]

Time (h)	Temperature (°C)	Phase Identified	Crystal Structure	a (Å)	c/a
16-1000	871	M_6C	cubic	10.95-11	-
16-1000	871	Co_2W	hexagonal	-	1.63
16-100	871	Zr(C, N)	cubic	4.56-4.6	-
16-100	871	$M_{23}C_6$	cubic	10.62	-

Still, recent research by Shingledecker, et. al. on a heat of Haynes® 25 with low silicon content shows improved ductility when compared to historical data from high silicon content heats. This suggests that Si may in fact play some role in the alloy's ductility loss.

In addition to the primary effect of the Laves phases, Wlodek outlined several ancillary effects which also caused embrittlement in Haynes® 25. First, he notes that the cobalt matrix in the alloy undergoes a FCC to HCP martensitic transformation at elevated temperatures, thus leading to a more brittle matrix. This effect was originally studied by Köster and has been confirmed by later research.[7,8] Second, the coarsening of the Laves phase may serve as a stress concentration site and therefore make it more prone to nucleating cracks.

Yukawa and Satô followed up on Wlodek's work by using diamond pyramid hardness testing to studying the effects of aging on hardness and stress rupture properties over a temperature range of 500 to 1100°C.[4] Like Wlodek, Yukawa and Satô conducted both x-ray and electron diffraction on the alloy. However, they observed seven unique precipitates as shown in Table 4. Most notably, Yukawa and Satô confirmed the presence and crystallographic description of the Laves phase. While they also agreed upon the presence and crystallography of the metal carbide phases, Yukawa and Satô did

Table 4. Phases reported by Yukawa and Satô[4]

Time (h)	Temperature (°C)	Phase Identified	Crystal Structure	a (Å)	c/a
0.3-7	700-800	M_7C_3	hexagonal	13.98	0.33
0.5-1000	700-800	$M_{23}C_6$	cubic	10.55-10.68	-
4-1000	700-800	M_6C	cubic	10.99-11.22	-
300-1000	700	α-Co_3W	L12-ordered fcc	3.57	-
300-1000	700	β-Co_3W	D019-ordered hexagonal	5.11	0.8
100-1000	800	Co_2W	C14 hexagonal	4.73	1.63
800-1000	800	μ-Co_7W_6	D85 hexagonal	4.73	5.39

not report any type of zirconium precipitate in their findings.

Yukawa and Satô were the first to propose the currently-accepted precipitation sequence in Haynes® 25. At 800°C:

$$M_7C_3 \rightarrow M_{23}C_6 \rightarrow M_6C \rightarrow Co_2W \rightarrow \mu\text{-}Co_7W_6$$

while at 700°C:

$$M_7C_3 \rightarrow M_{23}C_6 \rightarrow M_6C \rightarrow \alpha\text{-}Co_3W \rightarrow \beta\text{-}Co_3W \rightarrow Co_2W$$

where the italicized M_7C_3 and α-Co_3W phases are metastable. Yukawa and Satô summarized these precipitation reactions in a time-temperature transformation (TTT) diagram for Haynes® 25 which is replotted from their original work in Figure 1.

Yukawa and Satô also described the morphologies of the various precipitates in Haynes® 25. Of particular interest is the Laves Co_2W phase – its morphology was described as elongated platelets which coagulate and form large intergranular precipitates upon extended aging at 800°C. In contrast, the Laves phase occurs as fine particles after aging at 700°C. Most importantly, Yukawa and Satô reported that the Laves phase seemed to follow M_6C near grain boundaries. These findings lend further credence to the assertion by Wlodek that a precipitation reaction producing Laves-Co_2W on the grain boundaries is the primary cause for embrittlement in Haynes® 25.

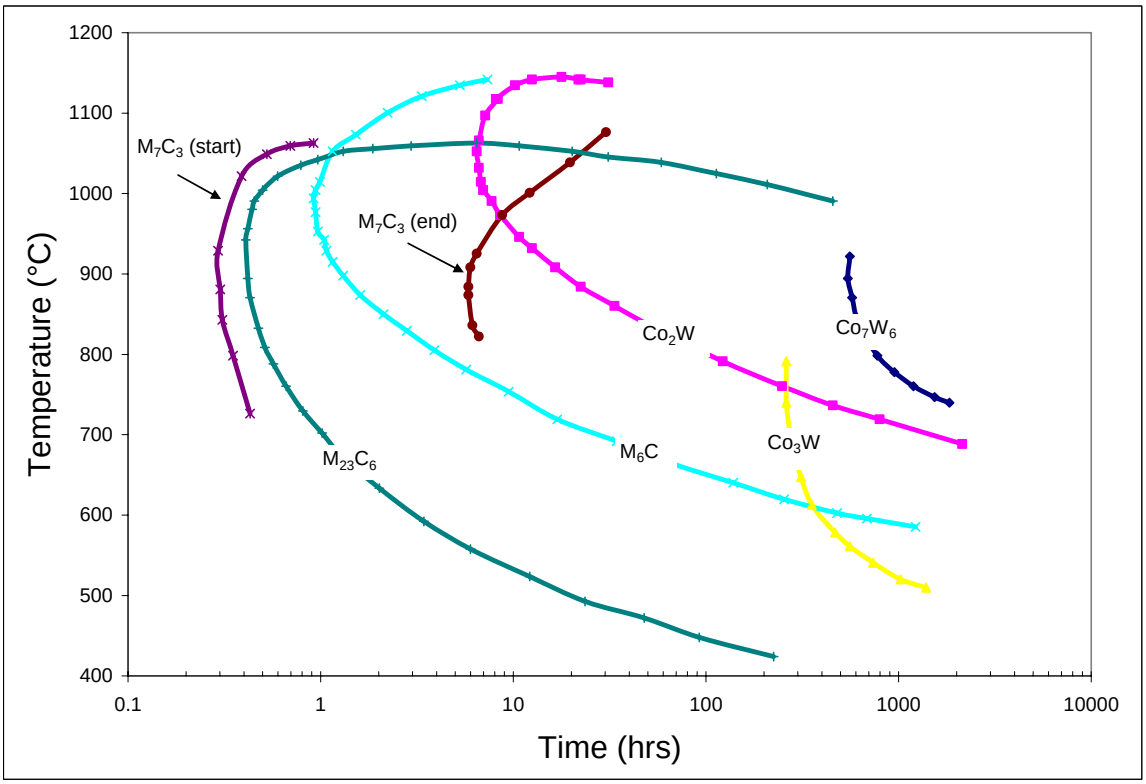

Figure 1: TTT Diagram for Haynes 25®, after Yukawa and Satô[4]

Bourgette employed Charpy impact and tensile testing to study the effects of aging on ductility in Haynes® 25.[5] He found that toughness decreased after aging at 870 and 760°C but remained relatively unchanged at aging temperatures of 650° and below. Bourgette describes his microstructural characterization techniques as "metallographic examination" and "chemical analysis," without providing any details. It is surmised here that they were optical microscopy and EDS via SEM, respectively. Using these techniques Bourgette was able to identify all of the phases previously reported by Yukawa and Satô, as shown below in Table 5. Most importantly, he reaffirmed previous assertions that the Laves-Co_2W is the primary reason for ductility loss in Haynes® 25 and notes that the Co_3W phase may also be responsible for ductility loss at temperatures too low for the formation of the Laves phase. Bourgette also noted the secondary effect of the Laves phase on the matrix. As the Laves phase first precipitates and then coarsens, the alloy becomes depleted in tungsten, thereby limiting its solid solution strengthening effect.

Hammond used x-ray diffraction as well as scanning electron microscopy to study the effects of aging on tensile ductility in Haynes® 25.[9] He successfully identified the

Table 5: Phases Reported by Bourgette[5]

Time (hrs)	Temperature (°C)	Phase Identified	Crystal Structure	a (Å)	c/a
50-4000	760-870	Co2W	-	-	-
100-4000	870	M6C	-	-	-
100-4000	870	M23C6	-	-	-
500	760	M7C3	-	-	-
500	760	α-Co3W	-	-	-
500	760	ß-Co3W	-	-	-

Laves Co_2W and carbide phases, but reported approximately 7.4 weight percent of an unidentified phase which he speculated was most likely the μ-Co_7W_6 phase identified by Yukawa and Satô. Ultimately, Hammond's results agreed with previous research – the Laves Co_2W phase causes brittle fracture, which in turn leads to a sharp loss in ductility in Haynes® 25. Because his research was more focused on the ductility of Haynes® 25, Hammond's microstructure findings are largely qualitative and are not tabulated here.

In contrast to these earlier studies, recent research by Teague et. al. have challenged the existence of a Laves phase in Haynes 25 after aging at 550-1000°C.[6] They studied the microstructure and mechanical properties of specimens that had been aged at temperatures ranging from 550 to 1000°C for times up to 8640 hours. Mechanical properties were studied via tensile testing. Both scanning and transmission electron microscopy failed to reveal the Laves and the Co_7W_6 phases reported in previous studies. They did, however, note the presence of α-Co_3W and confirmed Wlodek's report that the M_6C has the composition W_3Co_3C. Teague et al. proposed that coverage by this W_3Co_3C phase on the grain boundaries was the reason for embrittlement at temperatures between 800 and 100°C. At lower temperatures (600°C and below), Teague attributed the ductility loss to highly localized plasticity, which leads to shear fracture at low macroscopic strains. Teague et al.'s findings are shown in Table 6.

The most striking result of Teague et al.'s research is the apparent absence of the Laves Co_2W phase, which may be related to their TEM sample preparation technique. Previous research utilized very specialized electrolytic extraction and electro-polishing techniques. In contrast, Teague et al. used a jet electro-polishing apparatus for sample

Table 6. Phases reported by Teague et. al.[6]

Time (hrs)	Temperature (°C)	Phase Identified	Crystal Structure	a (Å)	c/a
2160	550	-	-	-	-
2160-8640	600-1000	M_6C	cubic	11.11	-
4320	800	α-Co3W	L12-ordered fcc	3.57	-

preparation. Due to the extremely brittle nature of the Laves phase, it is possible that this precipitate may have simply "fallen out" of the matrix during polishing.

McKamey and George employed tensile and impact testing to study the ductility loss in Haynes® 25 for aging times far greater than those in previous research.[10] Their research considered three aging temperatures – 550, 675, and 850°C – for aging times of up to 10,000 hours. At 850°C McKamey and George observed the previously-described drop in ductility at aging times consistent with the precipitation of the Laves phase in Yukawa and Satô's TTT diagram (Fig. 1). They also measured a more gradual loss in ductility at 675°C and no appreciable ductility decrease in specimens aged at 550°C.

Upon studying the microstructure using SEM, McKamey and George noticed bands of stacking faults in specimens aged at 675°C for extended times. These stacking faults may be associated with the fcc-to-hcp transformation that occurs in this alloy. At 850°C McKamey and George observed a blocky, tungsten-rich precipitate after aging for as little as 240 hours with large amounts of grain boundary coverage after aging for 10,000 hours. They also pointed out the difficulty in positively identifying phases in the SEM and the need for TEM to determine the chemistry and crystallographic structure of these precipitates.

George was the first to describe both the hardening and ductility loss in Haynes®

25 using an Avrami equation of the form

$$\frac{P - P_{\max}}{P_{\max} - P_{\min}} = 1 - e^{(kt^n)}$$

where P is the property of interest (hardness and ductility in this case), and k and t are kinetic constants. [11] Plots of the hardness and ductility loss are shown below in Figure 2 and Figure 3, respectively.

Recently, Shingledecker et. al. generated extensive mechanical properties data using creep and tensile testing. [12] Their research confirmed the loss in ductility in

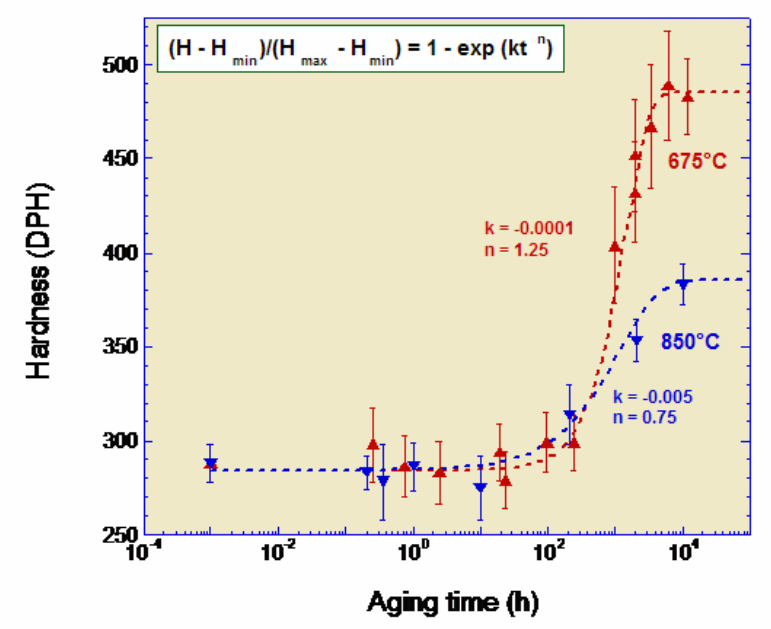

Figure 2: Hardness versus Aging Time[11]

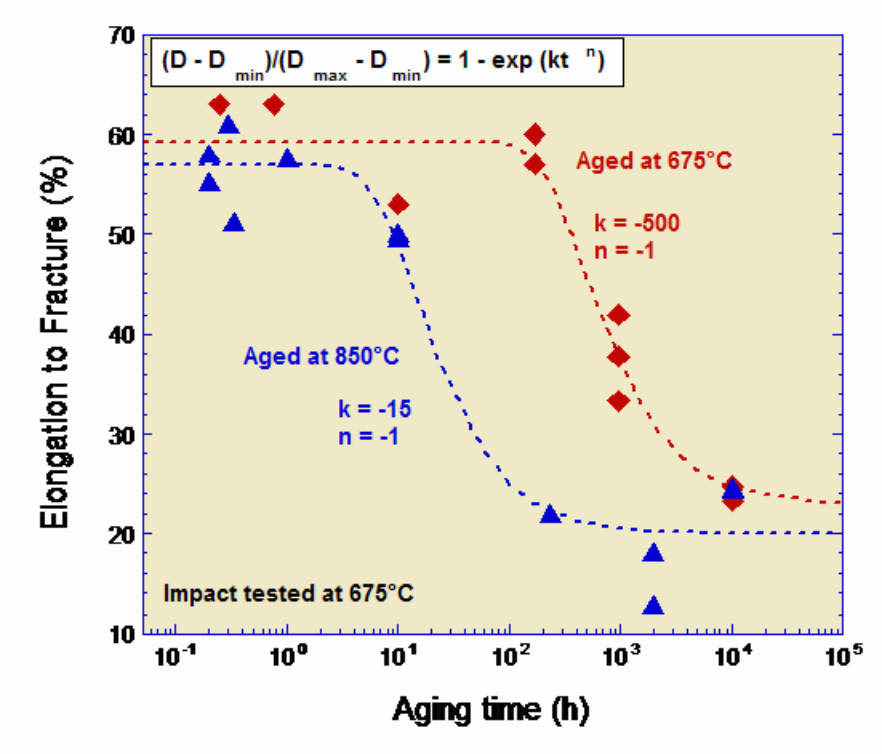

Figure 3: Ductility versus Aging Time[11]

Haynes® 25 upon aging at temperatures of 675°C and above for extended times. They were also able to quantify the loss in tensile elongation (EL) and reduction of area (RA) at room temperature and 650°C using an Avrami expression. The kinetic constants *k*, *t*, and *n* for this expression are listed in Table 7, and a ductility plot is shown in Figure 4.

An Avrami type description of ductility loss is important because it suggests that, while the mechanism for ductility loss is not yet fully understood, it may be related to increasing coverage of the grain boundaries by intermetallic precipitates, or increasing volume fraction of precipitates, with increasing aging time and temperature.

Table 7: 675°C Avrami Constants Reported by Shingledecker, et. al.[12]

Test Temp (°C)	Elongation		Reduction in Area	
	k	n	k	n
23	-515.15	-1.1835	-789.8	-1.228
650	-77.14	-0.737	-764.38	-0.9949

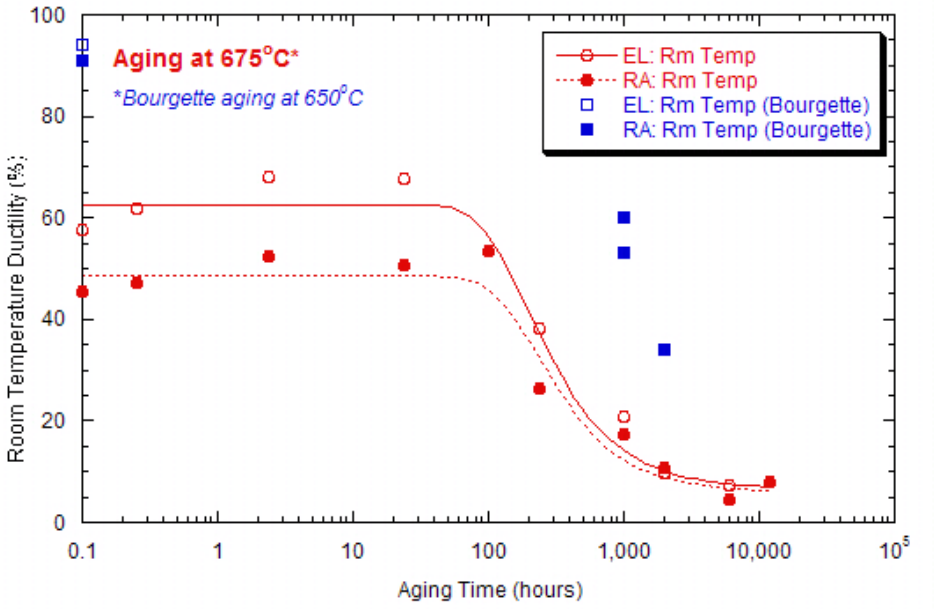

Figure 4: Room Temperature Elongation (EL) and Reduction of Area (RA) of Haynes® 25[12]

Problem Statement

Virtually all previous crystallographic data have been obtained by X-ray diffraction on extraction replicas, or by electron diffraction on replicas or thin foils. The majority of previous chemical compositions have been determined by electron diffraction, energy dispersive spectroscopy (EDS) in a scanning electron microscope (SEM), or by other electron microprobe techniques. While EDS in an SEM can be a valuable tool for qualitative chemical information, it generally should not be relied upon for quantitative chemical information due to potential volume effects.[13] To minimize these effects, EDS in a transmission electron microscope (TEM) is preferable.

The goal of this research was therefore two-fold. First, to perform a definitive study on the chemical composition of the various precipitates using more accurate techniques. Second, to examine the microstructure of Haynes® 25 and compare it to both historical and on-going mechanical tests in an attempt to develop empirical relationships between quantitative microstructural features and ductility loss.

Experimental Approach

Aging conditions were chosen such that each sample would contain at least one of the eight phases shown on the TTT diagram. Specimens were prepared for aging by placing them in an evacuated quartz tube which was then backfilled with argon. Two exceptions to this practice were made – the samples aged for 56.7 and 8,975 hours at 850°C were taken from the shoulder region (unstressed) of ruptured creep specimens. All of these materials were from the same heat of material studied by McKamey and George and Shingledecker et. al. These specimens were examined and characterized with the aid of either SEM or TEM. Table 8 and Table 9 show a summary of all specimens and the analysis methods used to study each.

Samples for SEM observation were taken from one corner of each specimen and mounted in epoxy. The sample was then ground flat and polished using progressively finer diamond pastes until a 1 μm polish was attained. The SEM was performed using an FEI/Philips XL-30 FEG-SEM. Images of grain boundaries were taken, and a linear fraction of grain boundary coverage by precipitates was calculated using Scion Image, a

Table 8: Summary of Specimens Aged at 675°C

Aged at 675°C		Analysis Type	
		SEM	TEM
Aging Time (h)	0.25	x	x
	24	x	
	240	x	
	1000	x	
	2000	x	
	6000	x	x
	12000	x	x

Table 9: Summary of Specimens Aged at 850°C

Aged at 850°C		Analysis Type	
		SEM	TEM
Aging Time (h)	0.33	x	x
	0.75	x	
	1	x	
	9.5	x	
	57.6*	x	
	2000	x	x
	8975*	x	x
*samples aged in air			

digital imaging software program. To perform this calculation, the total length of grain boundaries in each image was first measured and recorded. Then, the length of each precipitate which intersects a grain boundary (i.e. is "on" the grain boundary) was measured and recorded. Within a given sample there was some variation in precipitate coverage from one grain boundary to the next, therefore four images were analyzed for each aging condition. The lengths from each image were summed and divided by the total grain boundary length to obtain the linear fraction of coverage. A diagram of grain boundary coverage measurements is shown in Figure 5. The equation for linear fraction of coverage (f) is given by the equation:

$$f = \frac{l_1 + l_2 + \ldots l_i}{L}$$

Grain boundary precipitate diameter was also measured using Scion Image and, for the purpose of this study, is defined as the average precipitate size.

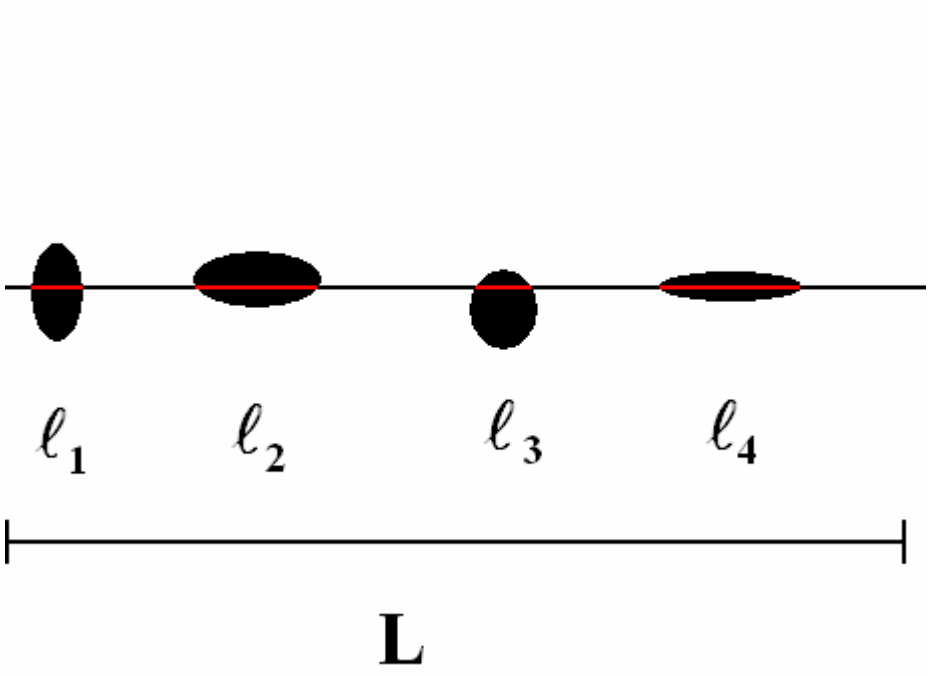

Figure 5: Diagram of Grain Boundary Coverage Measurement

Samples for examination in the TEM were also taken from specimen corners. Extraction replicas were made by first etching with a solution of 7% sulfuric acid in methanol at a 5 volt potential for roughly 30 seconds. The etched samples were then coated with a copper film and the precipitates extracted using methyl sulfuric acid at 16 volts for 4 to 5 minutes. TEM work was performed in an FEI/ Tecnai 20T TEM operating at 200kV with an EDS detector resolution of between 140 and 160 electron-volts. EDS was performed to determine precipitate chemistry, and the resulting spectra were analyzed using the standardless analysis feature in ES Vision software. TEM foils were also prepared using jet electro-polishing. However, examination of these foils in the TEM revealed that the precipitates of interest had "fallen out" of the matrix during sample preparation.

Results and Discussion

Aging at 675°C

Figure 6 shows SEM micrographs of Haynes® 25 aged at 675°C. These images show a fine distribution of grain boundary precipitates, which appear after 1,000 hours and increase in number density and fraction with aging time. Very little precipitation is observed in the matrix except for the occasional coarse primary carbide. However, after 6,000 hours of aging the presence of what appear to be stacking faults is noted. These stacking faults are likely related to the fcc-to-hcp transformation which is known to occur at this temperature.[8] Attempts to characterize the chemistry of the grain boundary precipitates at 675°C using TEM were unsuccessful as the TEM replicas only captured the larger matrix precipitates. Figure 7 shows a TEM micrograph of Haynes® 25 aged for 6000 hours. Figure 8 and Figure 9 show EDS data of the matrix precipitates. The gray precipitates have the composition $(Cr_{19}W_2Co_{1.5}Fe_{0.5})C_6$ which is consistent with the $M_{23}C_6$ phase while the black precipitates are consistent with the M_6C phase and have a composition of $W_3Co_{1.5}Cr_{1.5}C$ (for complete tabular EDS data please reference Appendix B). These dark precipitates have a composition similar to that of the grain boundary precipitates shown in the SEM micrographs in Figure 6.

In order to correlate ductility loss with microstructure, the linear fractional coverage of the grain boundaries by precipitates was measured. The results of these measurements are shown graphically in Figure 10. These data can be found in tabular form in appendix A.

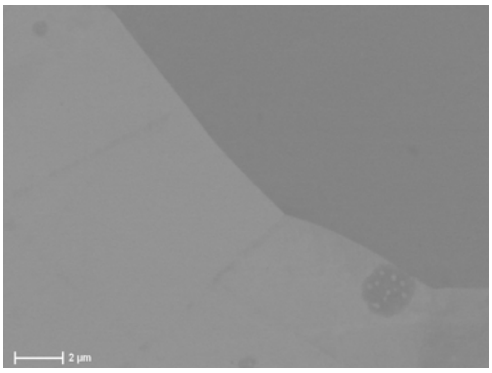

(a)

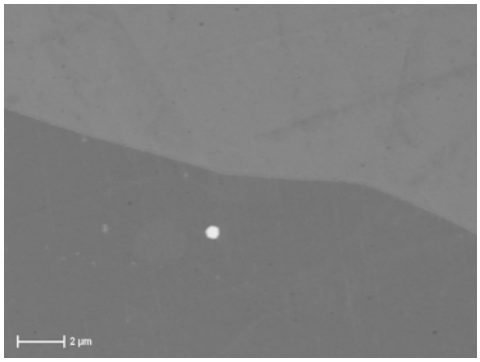

(b)

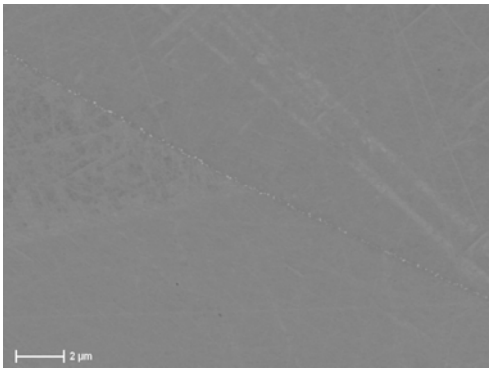

(c)

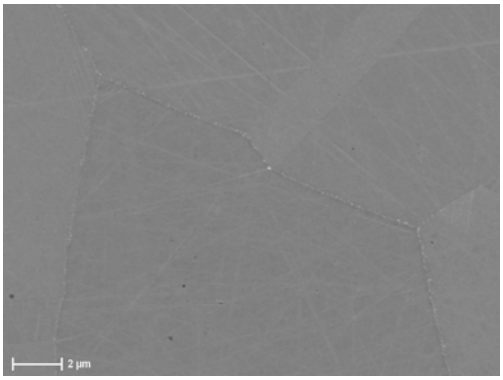

(d)

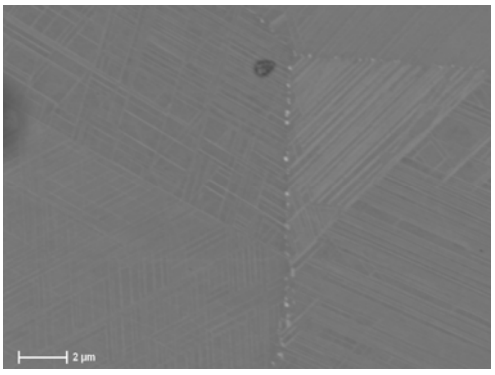

(e)

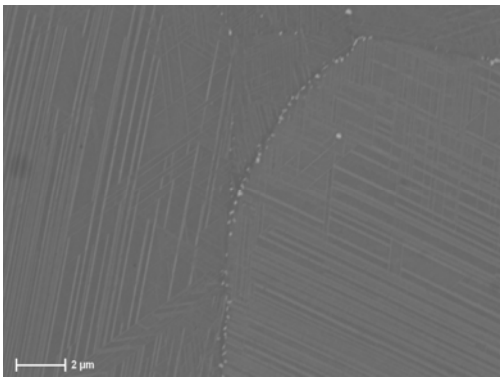

(f)

Figure 6: Haynes 25 Aged at 675°C for (a) 2.4h, (b) 24h, (c) 1000h, (d) 2000h, (e) 6000h, and (f) 12000h

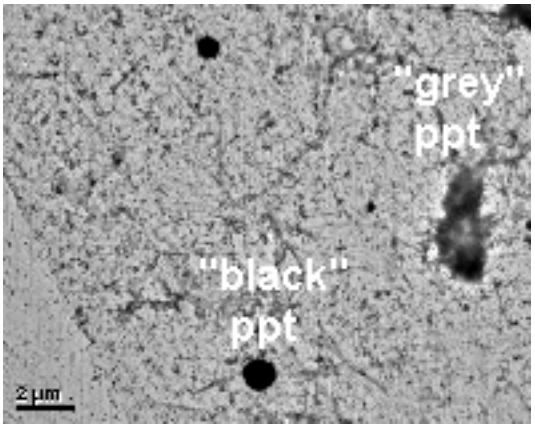

Figure 7: TEM Micrograph (extraction replica) of Haynes 25 precipitates after aging for 6000h at 675°C

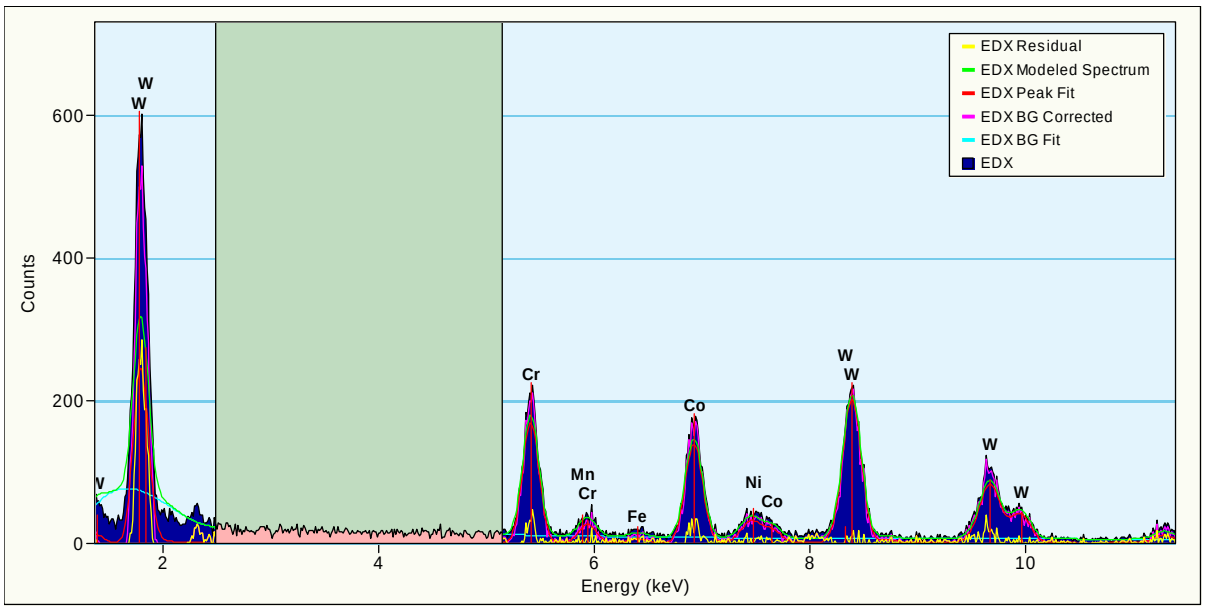

Figure 8: EDS Spectrum of Black Precipitates

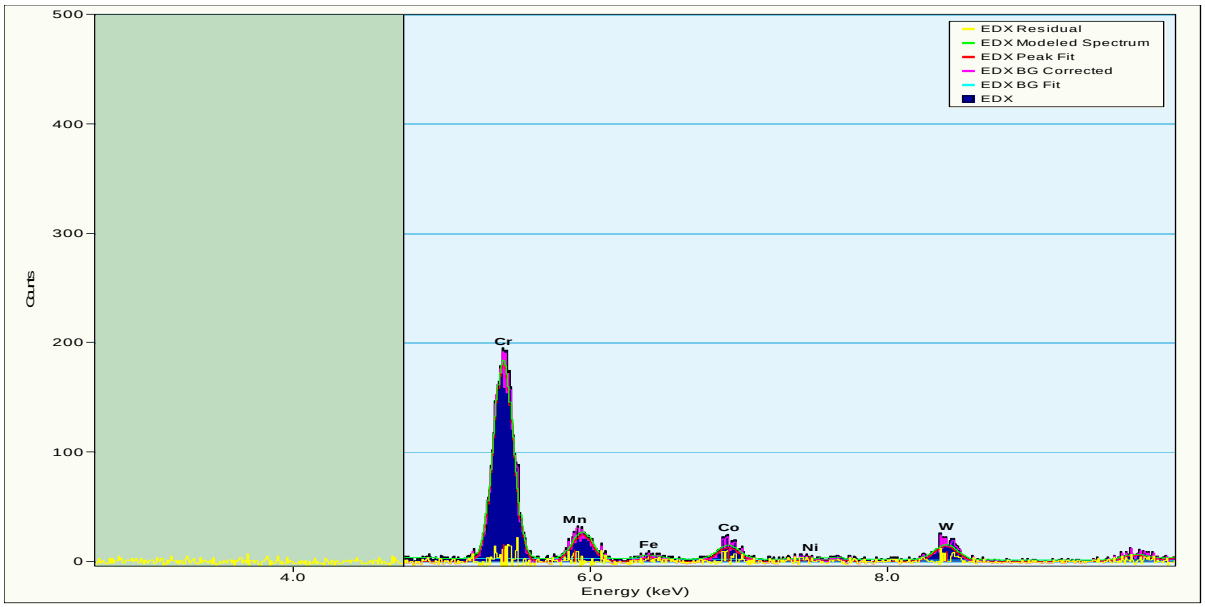

Figure 9: EDS Spectrum of Gray Precipitate

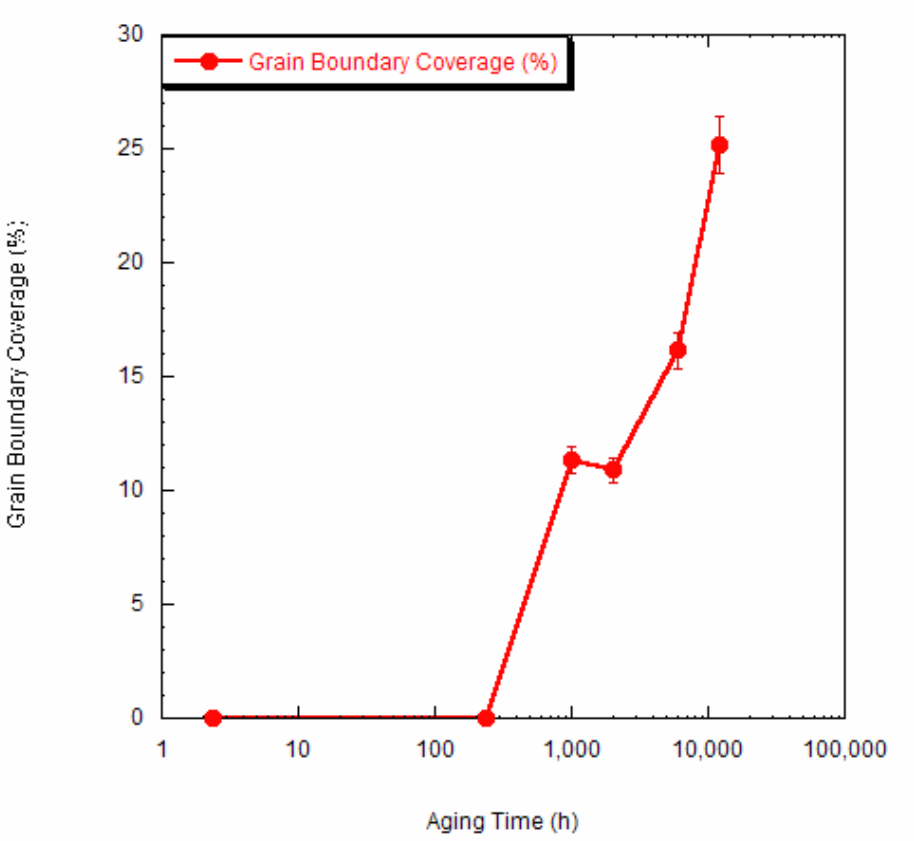

Figure 10: Linear Fractional Grain Boundary Coverage on Aging at 675°C

Qualitatively, there is a large initial change in grain boundary coverage after aging for 1,000 hours with very little difference in the grain boundary microstructure after aging times greater than 6,000 hours which suggests that grain boundary coverage may not be the primary cause for embrittlement at this temperature. Another possible explanation for the lack of grain boundary precipitates after short aging times is the lack of spatial resolution provided by SEM – the grain boundary precipitates may simply be too small to be viewed and resolved. The graph in Figure 11 suggests that ductility begins to decrease well before the fractional grain boundary coverage begins to change. Tabular ductility data is also given below in Table 10.

Figure 12 shows the change in grain boundary precipitate size as a function of aging temperature. As expected, the precipitates coarsen over time. In order to correlate ductility loss and precipitate size, the two were first plotted versus aging time and then versus each other as shown in Figure 13 and Figure 14, respectively. While there appears to be a similar general trend for ductility and precipitate size in Figure 13, the two do not appear to be directly related. This would suggest that while grain boundary coverage may have an effect on ductility at 675°C, it is not the main cause. Instead, it is very likely that the fcc-to-hcp transformation which is known to occur in this temperature range may be the primary effect.

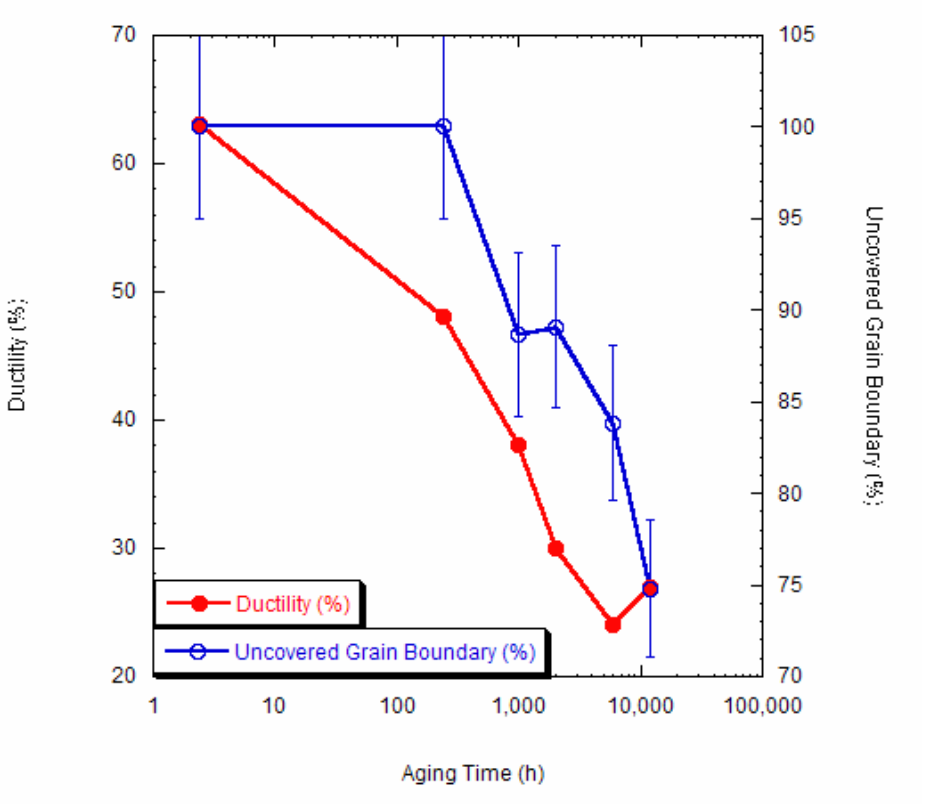

Figure 11: Ductility and Percent Uncovered Grain Boundary versus Aging Time at 675°C

Table 10: Tensile Impact Elongation Data for Aging at 675°C[9]

Aging Time at 675°C (h)	Elongation to fracture (%)
2.4	63
240	48
1000	38
2000	30
6000	24
12000	27

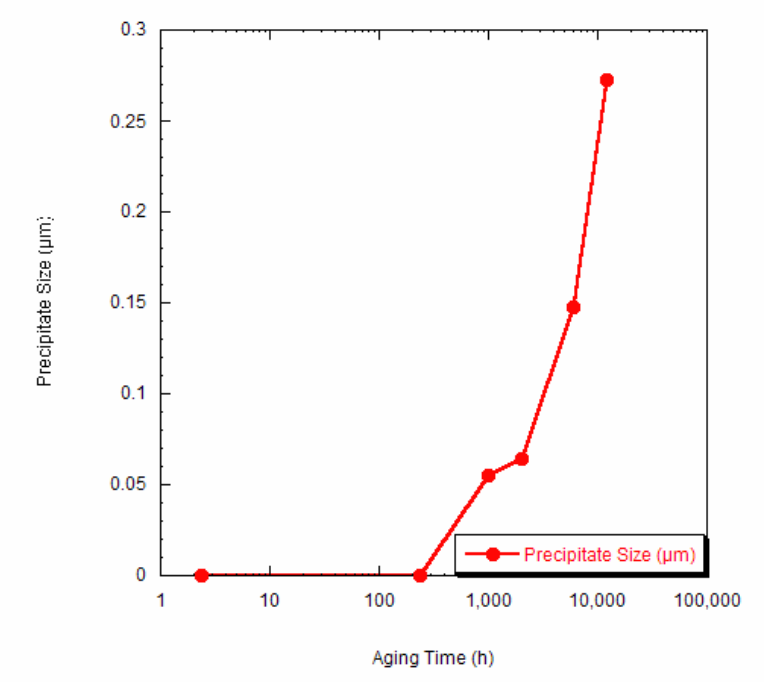

Figure 12: Precipitate Size versus Aging Time at 675°C

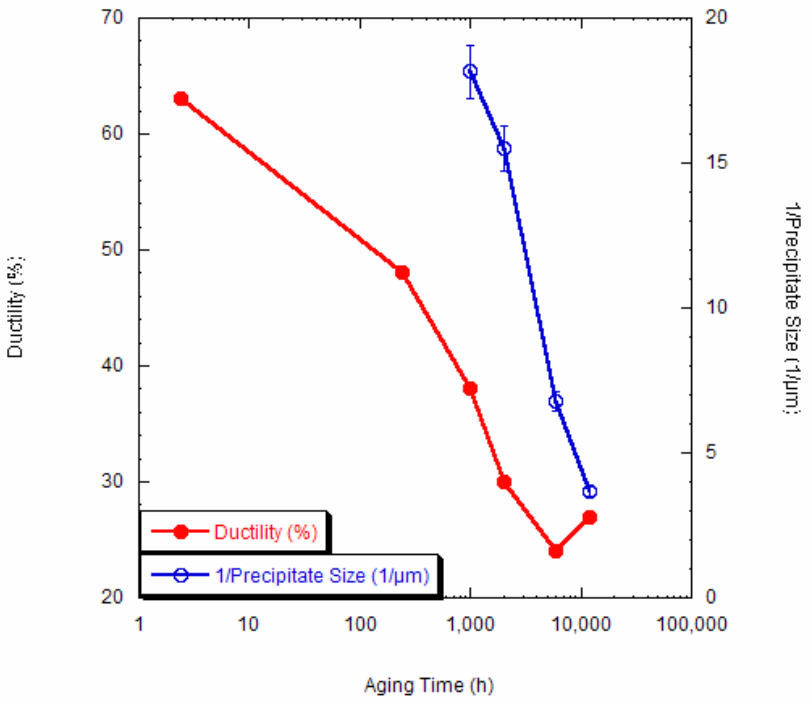

Figure 13: Ductility and Precipitate Size versus Aging Time at 675°C

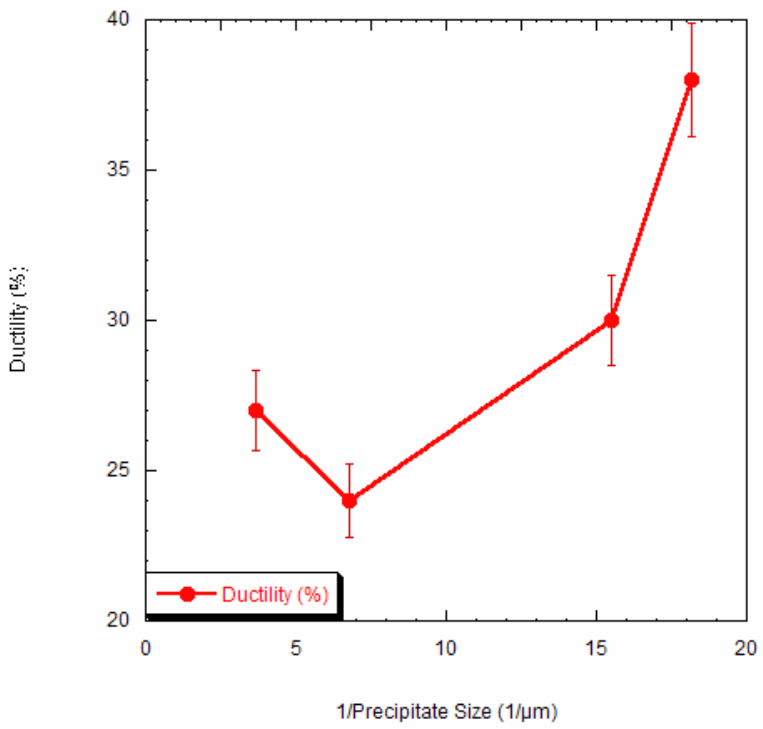

Figure 14: Ductility versus Precipitate Size on Aging at 675°C

Aging at 850°C

Figure 15 shows SEM micrographs of Haynes® 25 aged at 850°C. Qualitatively, these samples show grain boundary precipitation after a very short time with extensive grain boundary and matrix precipitation occurring at aging times of 2,000 hours and longer. After 8,975 hours of aging the appearance of plate-like precipitates occurs in the matrix at regions of varying contrast. These precipitates may denote the location of stacking faults in the matrix.

Samples at this aging temperature were successfully characterized as the TEM replicas captured the grain boundary precipitates. Figure 16 and Figure 17 show TEM micrographs of Haynes® 25 aged for 57.6 and 8975 hours respectively. Figure 18 and Figure 19 show EDS data of the matrix precipitates. The gray matrix precipitates again

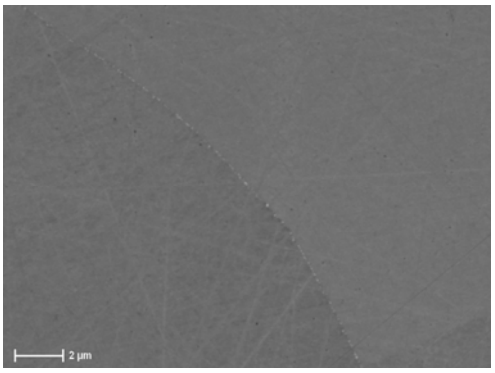

(a)

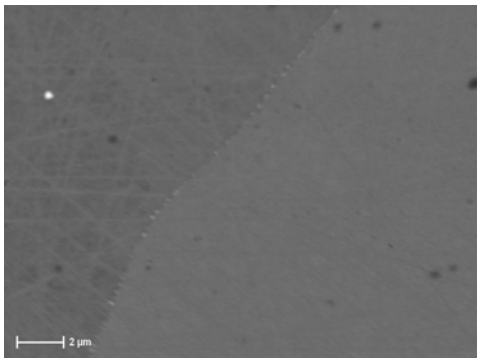

(b)

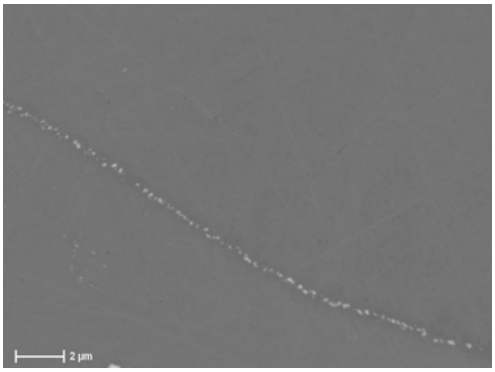

(c)

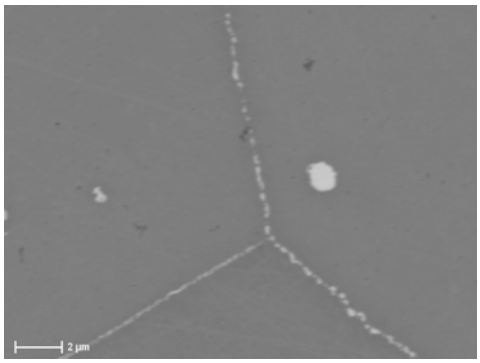

(d)

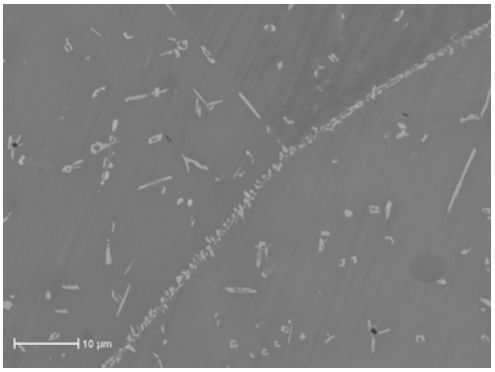

(e)

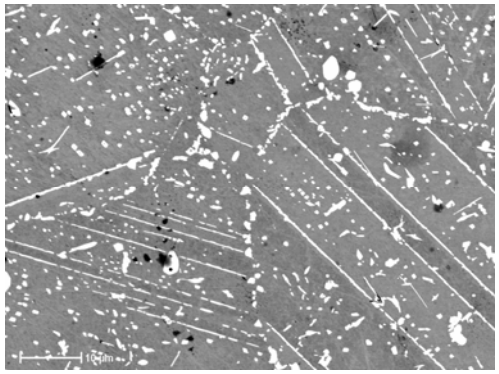

(f)

Figure 15: SEM Micrographs of Haynes 25 Aged at 850°C for (a) 0.33h, (b) 1h, (c) 9.5h, (d) 57.6h, (e) 2000h, and (f) 8975h

have the composition $(Cr_{19}W_2Co_{1.5}Fe_{0.5})C_6$ and are thus consistent with $M_{23}C_6$ while the black grain boundary precipitates have the composition $W_3Co_{1.5}Cr_{1.5}$ and are most likely M_6C (complete tabular EDS data can be found in Appendix B).

The first and most important result of this data is the absence of the Laves phase in the microstructure. While this phase has been reported in previous research and is generally accepted on the Haynes® 25 TTT diagram, no phase with a similar chemistry or crystal structure consistent with the Laves Co_2W or Co_7W_6 was ever observed or identified either by SEM-EDS or TEM-EDS/Diffraction. One reason for the absence of Laves phase is to the differences in chemistry of this heat of Haynes® 25 compared to the historical heats– the first heats of this material contained up to one percent silicon and much higher iron contents, both of which were thought to stabilize the Laves phase. For example, the range of Si levels in Wlodek's heats ranged from 0.37 to 0.91 weight percent while Fe levels ranged from 1.56 to 3.12 weight percent.[3]

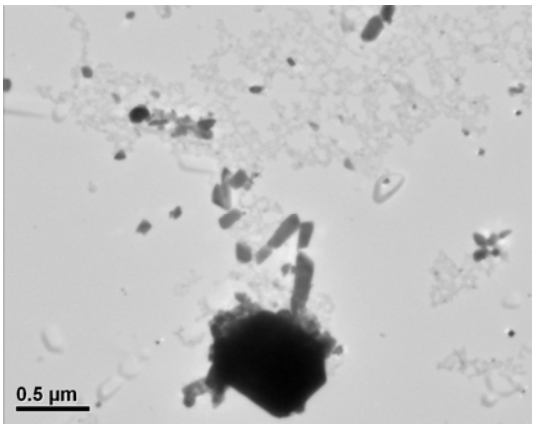

Figure 16: TEM Micrograph (extraction replica) of Haynes® 25 precipitates after Aging 57.6h at 850°C

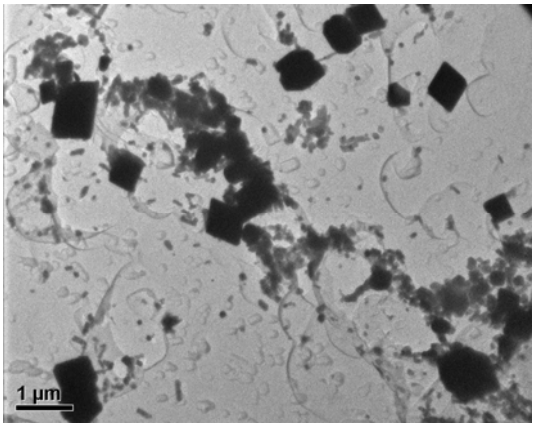

Figure 17: TEM Micrograph (extraction replica) of Haynes® 25 precipitates after Aging 8975h at 850°C

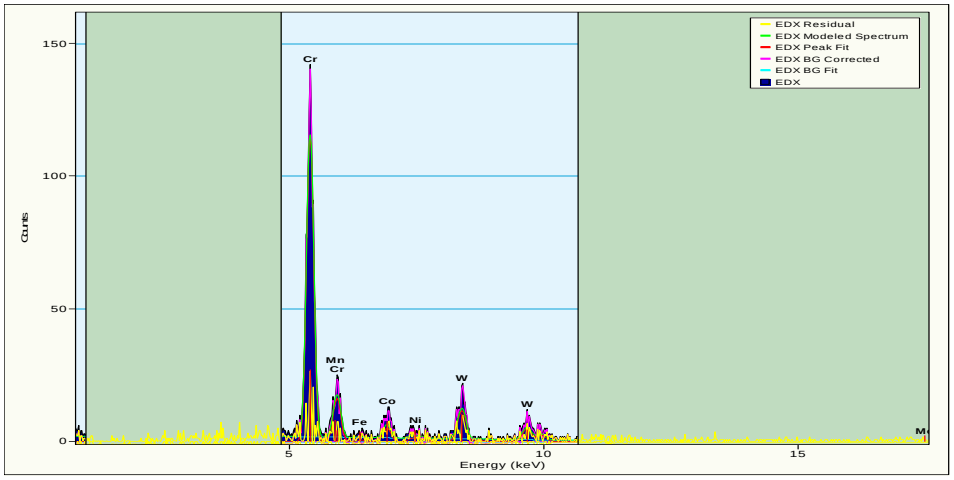

Figure 18: EDS Spectrum of "gray" precipitates

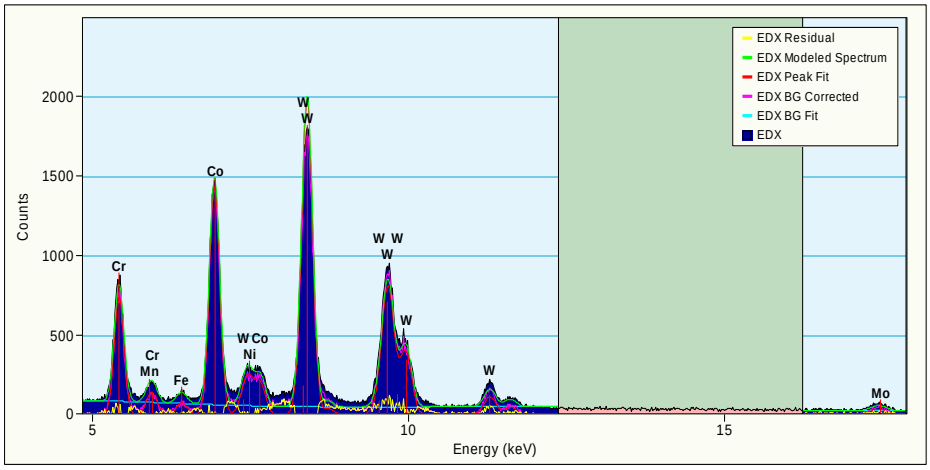

Figure 19: EDS Spectrum of "black" precipitates

As with the 675°C aging, the linear fractional coverage of the grain boundaries by precipitates was measured. Tabular grain boundary coverage data is located in Appendix A. Tabular ductility data is shown below in

Table 11. The results of these measurements are shown graphically in Figure 20. The graph in Figure 21 shows better agreement between the amount of uncovered grain boundary and the decrease in ductility at 850°C than at 675°C. Ductility and percent uncovered grain boundary concurrently drop with increasing time.

Figure 22 shows precipitate size versus aging time, which again verifies the coarsening behavior. Precipitate size and ductility were plotted versus aging time as shown in Figure 23 and versus each other as shown in Figure 24 in order to determine their relationship, if any, at 850°C. The results in Figure 23 show that there is a strong correlation between grain boundary coverage and ductility loss at 850°C. Figure 24 suggests an even stronger relationship between precipitate size and ductility loss at this temperature.

Table 11: Tensile Impact Elongation Data for aging at 850°C

Aging Time at 850°C (h)	Elongation to fracture (%)
0.33	56
9.5	50
57.6	23*
2015	16
8975	24*
*Interpolated from referenced ductility data	

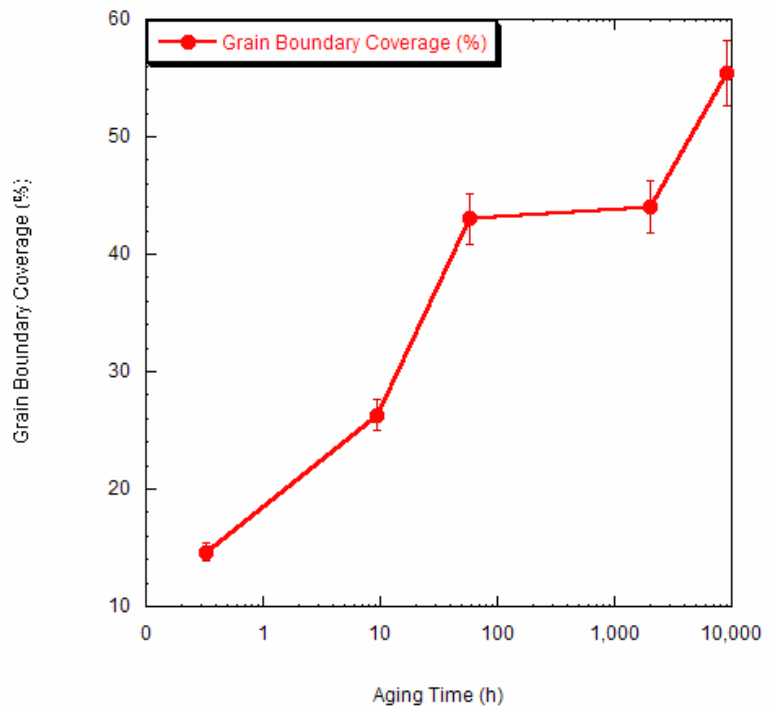

Figure 20: Linear Fractional Grain Boundary Coverage on Aging at 850°C

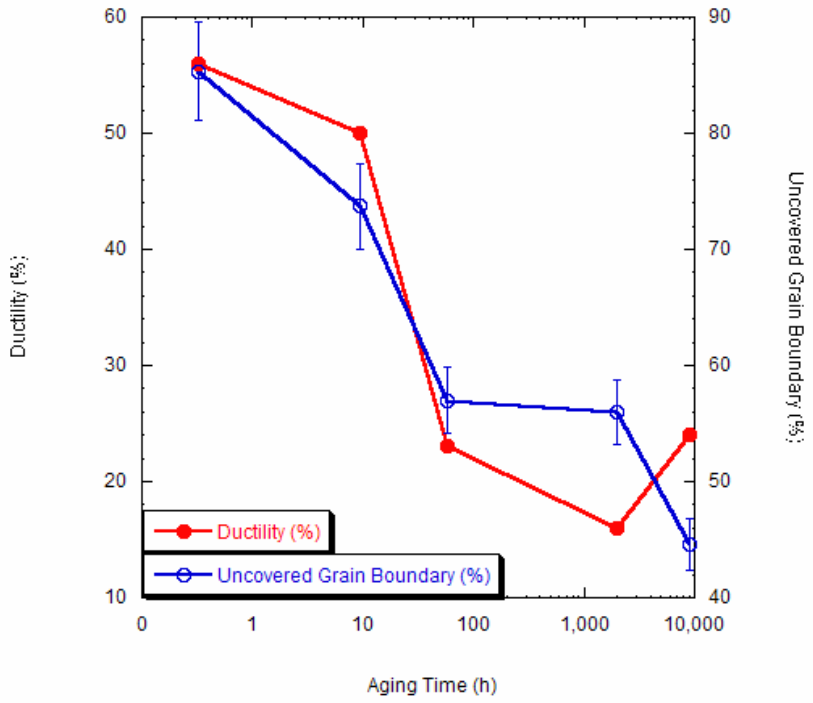

Figure 21: Ductility and Percent Uncovered Grain Boundary versus Aging Time at 850°C

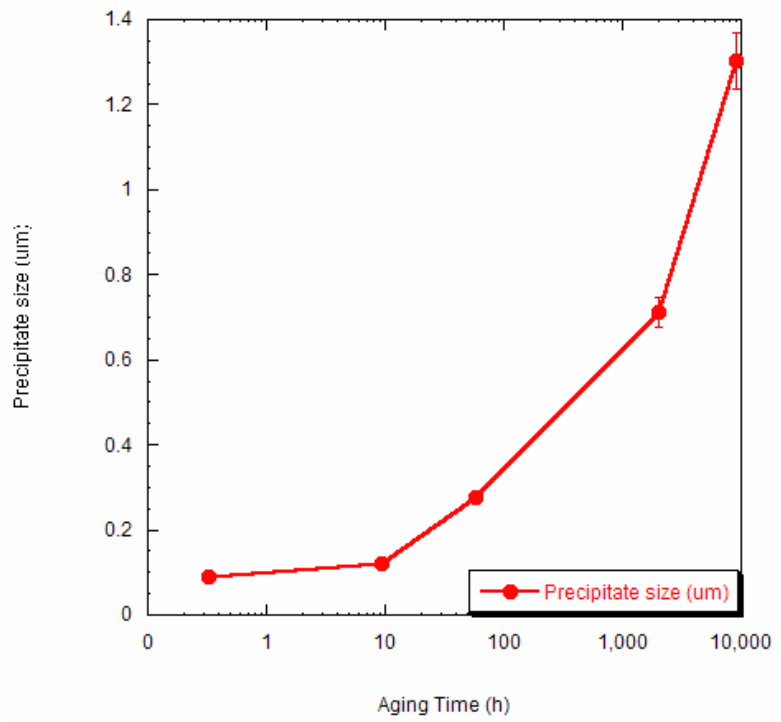

Figure 22: Precipitate Size versus Aging Time

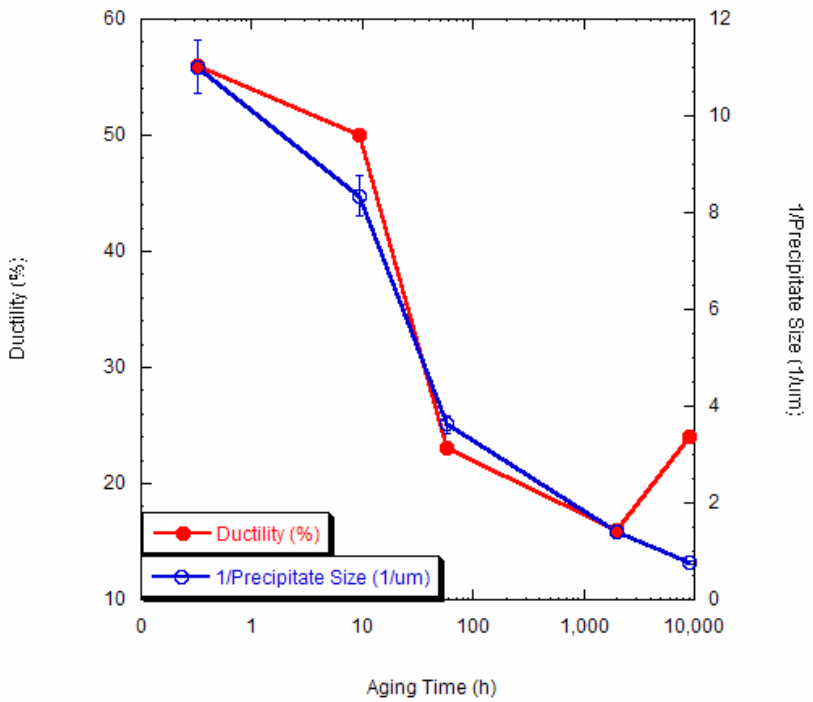

Figure 23: Ductility and Precipitate Size versus Aging Time at 850°C

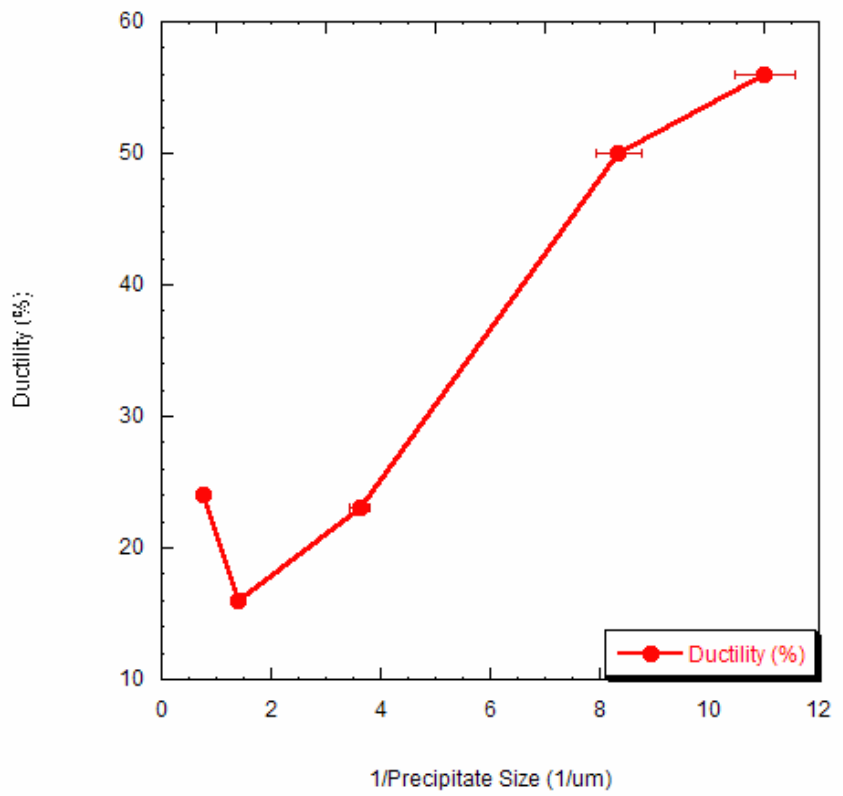

Figure 24: Ductility versus Precipitate Size on Aging at 850°C

Future Work

In order to confirm the proposition that the fcc-to-hcp transformation is the dominate cause for ductility loss at 675°C, it would be useful to attempt to measure the change in percent of hcp phase present after aging at various temperatures. In-situ SEM and X-ray diffraction should also be performed to better understand the precipitation kinetics for shorter aging times. With the difficulty in obtaining electron diffraction patterns in the TEM and the highly dubious nature of EDS data generated via SEM, it would be useful to obtain crystallographic data for the often small grain boundary precipitates. Electron backscatter diffraction presents itself as a useful tool in this area.

Finally, while there is an apparent correlation between grain boundary precipitation and ductility loss in the alloy, the underlying mechanism is still not fully understood. A more thorough TEM study on samples prepared with a focused ion beam (FIBS) technique would allow for imaging and study of the grain boundary-precipitate interface, which is believed to be weaker than the grain boundary-grain boundary interface.

Conclusion

Both scanning and transmission electron microscopy proved very useful in the characterization of aged Haynes® 25 specimens. EDS analysis of TEM replicas only identified two phases – the $M_{23}C_6$ phase with chemistry $(Cr_{19}W_2Co_{1.5}Fe_{0.5})C_6$ and the M_6C phase with chemistry $W_3Co_{1.5}Cr_{1.5}$. This M_6C phase was the predominant grain boundary precipitate in the alloy. No Laves-type Co_2W phase was identified in any of the analyzed specimens.

In summary, there appear to be two separate effects responsible for the ductility loss in Haynes® 25 on aging at 675°C and 850°C. At 675°C the fraction of uncovered grain boundary length has the correct general trend as ductility, but the two curves do not show enough similarity, there is a drop in ductility without evidence of any grain boundary precipitation, to make any concrete correlation between grain boundary precipitates and ductility loss. Instead, it is probably that the fcc-to-hcp transformation is also affecting the ductility at this temperature.

At 850°C there is a much closer correlation between grain boundary coverage and ductility loss – the two curves have very similar characteristics, and both appear to change at similar time values. Therefore, ductility loss in Haynes®25 on aging at 850°C may adequately be described to a first approximation using the linear fraction of covered (or, more accurately, uncovered) grain boundary.

References

1. "Haynes® 25 alloy Product Brochure." H-3057D, 2004 Haynes, Intl., www.haynesintl.com.

2. E.F. Bradley. Superalloys: A Technical Guide. ASM International, Metals Park, OH, 1988.

3. S.T. Wlodek. "Embrittlement of a Co-Cr-W (L-605) Alloy," *Trans. ASM*, American Society for Metals, 56, pp. 287-303, 1963.

4. N. Yukawa and K. Satô. "The Correlation between Microstructure and Stress-Rupture Properties of a Co-Cr-Ni-W (HS-25_ Alloy," pp. 680-686 in Proceedings of the International Conference on the Strength of Metals and Alloys, The Japan Institute of Metals, Omachi, Japan, 1968

5. D.T. Bourgette. "Effect of Aging Time and Temperature on the Impact and Tensile Behavior of L-605 – A Cobalt Base Alloy," ORNL-TM-3734, Oak Ridge National Laboratory, Oak Ridge, TN, 1973.

6. J. Teague, E. Cerreta, and M. Stout. "Tensile Properties and Microstructure of Haynes 25 Alloy after Aging at Elevated Temperatures for Extended Times," *Metallurgical and Materials Transactions A,* 35A (2004) pp. 2767-2781.

7. W. Köster. "On the Influence of the Elements on the Polymorphic Transformation of Cobalt." *Z. Metalkunde,* 43, p. 297, 1952.

8. H. L. Tawancy. "On the fcc → hcp transformation in a cobalt-base superalloy (Haynes alloy No. 25). *J. Mater. Sci.* Vol. 35 No. 3 (1986) pp. 337-341.

9. J. P. Hammond, "The Ductility Minimum and its Reversal with Aging in Cobalt-Base Superalloys," ORNL/TM-6624, Oak Ridge National Laboratory, Oak Ridge, TN.

10. C. McKamey and E. George. "Mechanical Properties of Haynes Alloy 25 Before and After Aging at 550-850°C." *Attachment to letter No. 0706-14-05, J.F. King to John Dowicki, July 8, 2005.*

11. E. George. Unpublished data.

12. J. P. Shingledecker, et. al. "Tensile and Creep-Rupture Evaluation of a New Heat of Haynes Alloy 25." ORNL/TM-2006/609. Oak Ridge National Laboratory, Oak Ridge, TN.

13. J. Goldstein, et. al. Scanning Electron Microscopy and X-Ray Microanalysis. 3rd Ed. Kluwer Academic/Plenum Publishers, New York, NY, 2003.

Appendices

The appendix is divided into two sections. The first section, Appendix A, provides SEM images of grain boundaries at various aging conditions and tabular results of the grain coverage measurements. The second section, Appendix B, provides TEM images along with EDS spectra and a summary table of the EDS analysis results. Note that EDS spectra for some probe points are not listed (e.g. ".r3_p2" for the 6000 hours at 675°C image). These spectra were omitted both here and in analysis due to the inability to obtain an EDS spectrum.

Appendix A

Aged 2.4h at 675°C

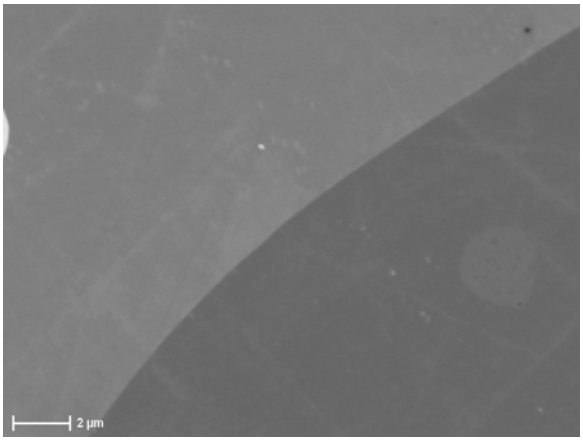

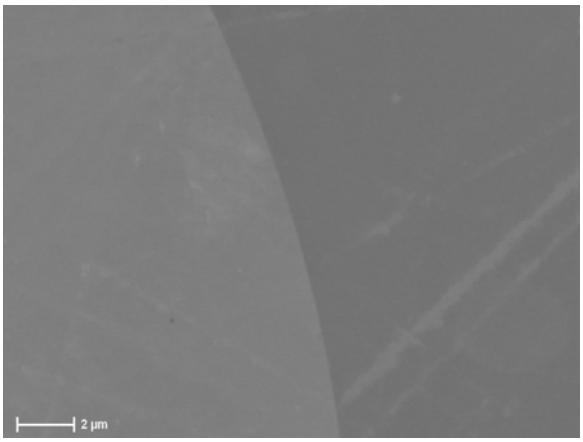

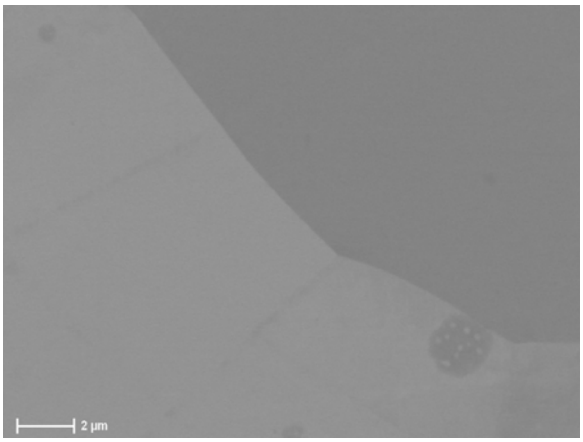

No grain boundary measurements performed due to absence of precipitates

Aged 240h at 675°C

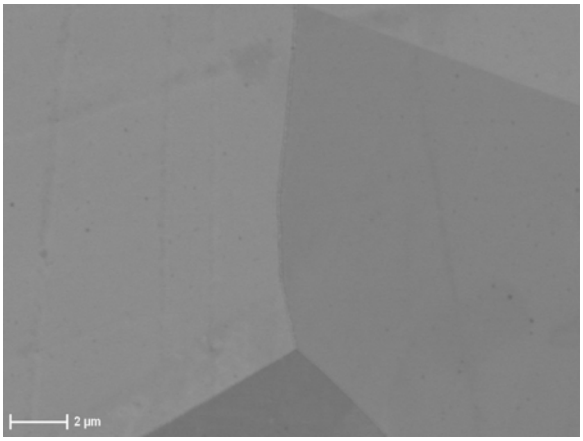

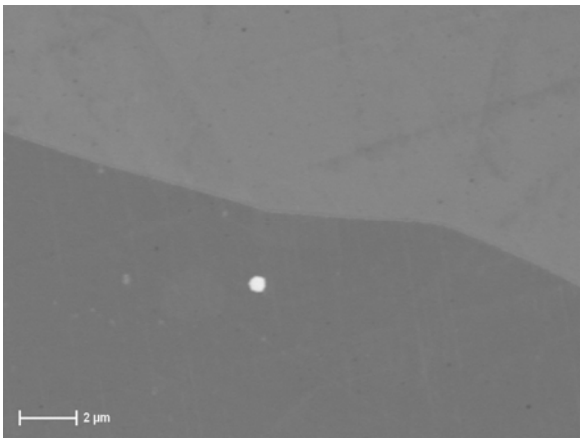

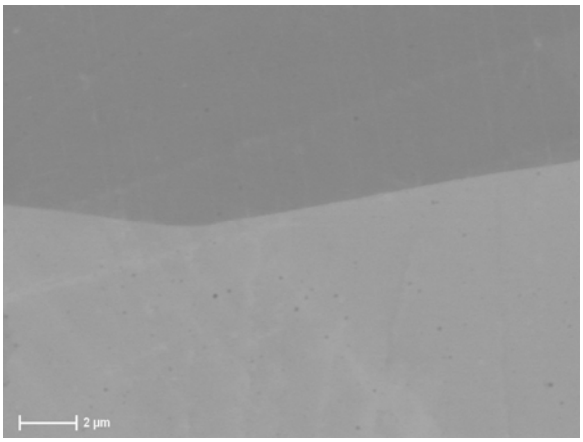

No grain boundary measurements performed due to absence of precipitates

Aged 1000h at 675°C

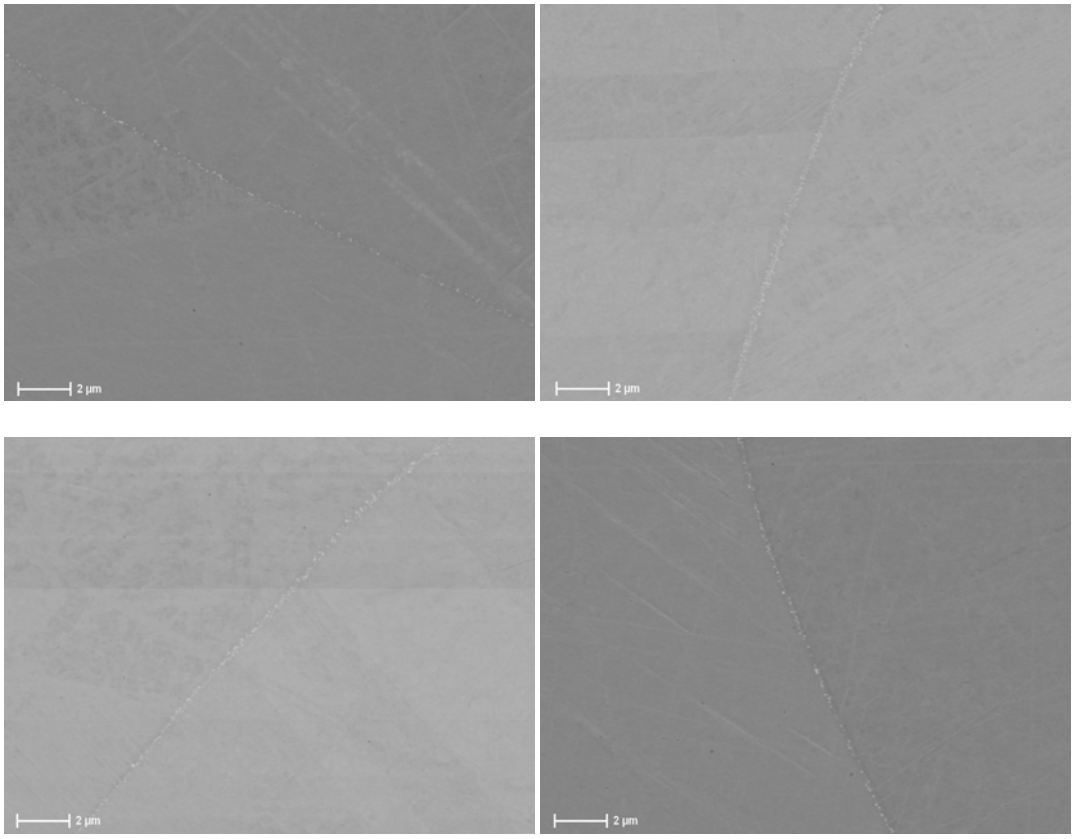

Image	Coverage	Average Size (µm^2)
64976	0.1097	0.0591
64977	0.1307	0.0457
64978	0.1089	0.0605
64979	0.1035	0.0551
Average	**0.1132**	**0.0551**
Standard Deviation	**0.1387**	**0.2177**
Standard Error	**0.0694**	**0.1089**

Aged 2000h at 675°C

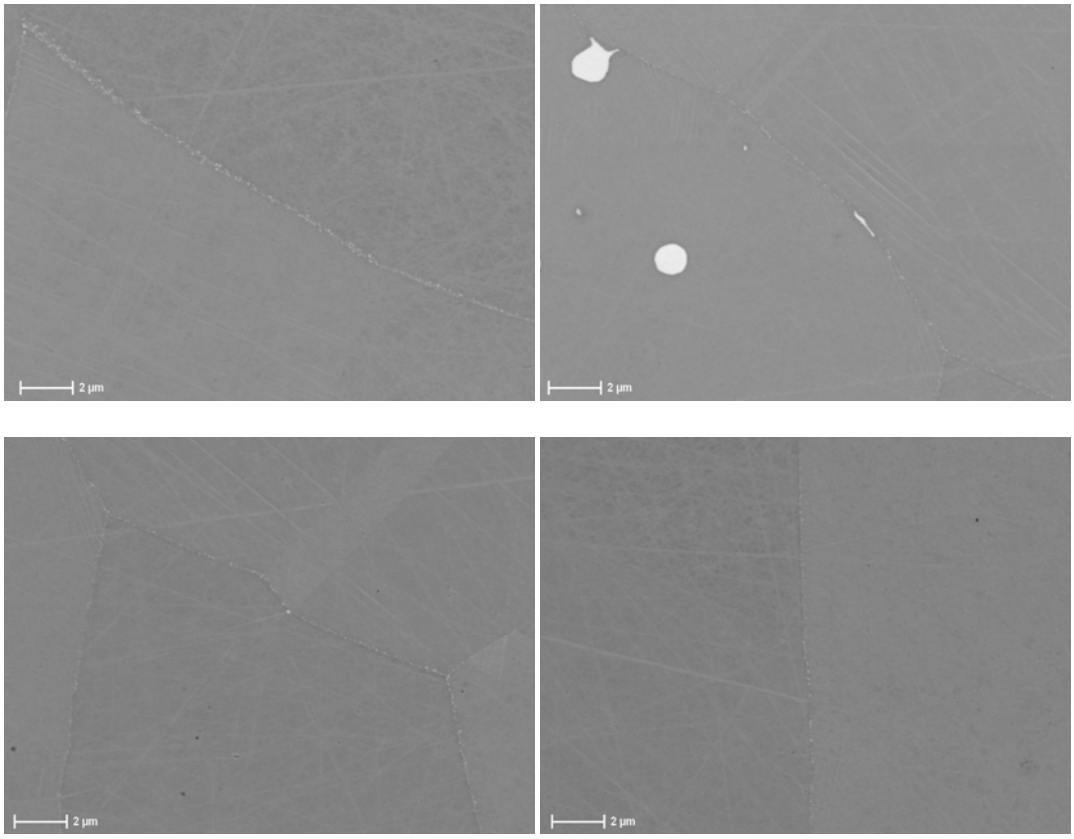

Image	Coverage	Average Size (µm^2)
64972	0.0903	0.0588
64973	0.1493	0.0943
64974	0.1189	0.0650
64975	0.0772	0.0403
Average	**0.1090**	**0.0646**
Standard Deviation	**0.1430**	**0.2082**
Standard Error	**0.0715**	**0.1041**

Aged 6000h at 675°C

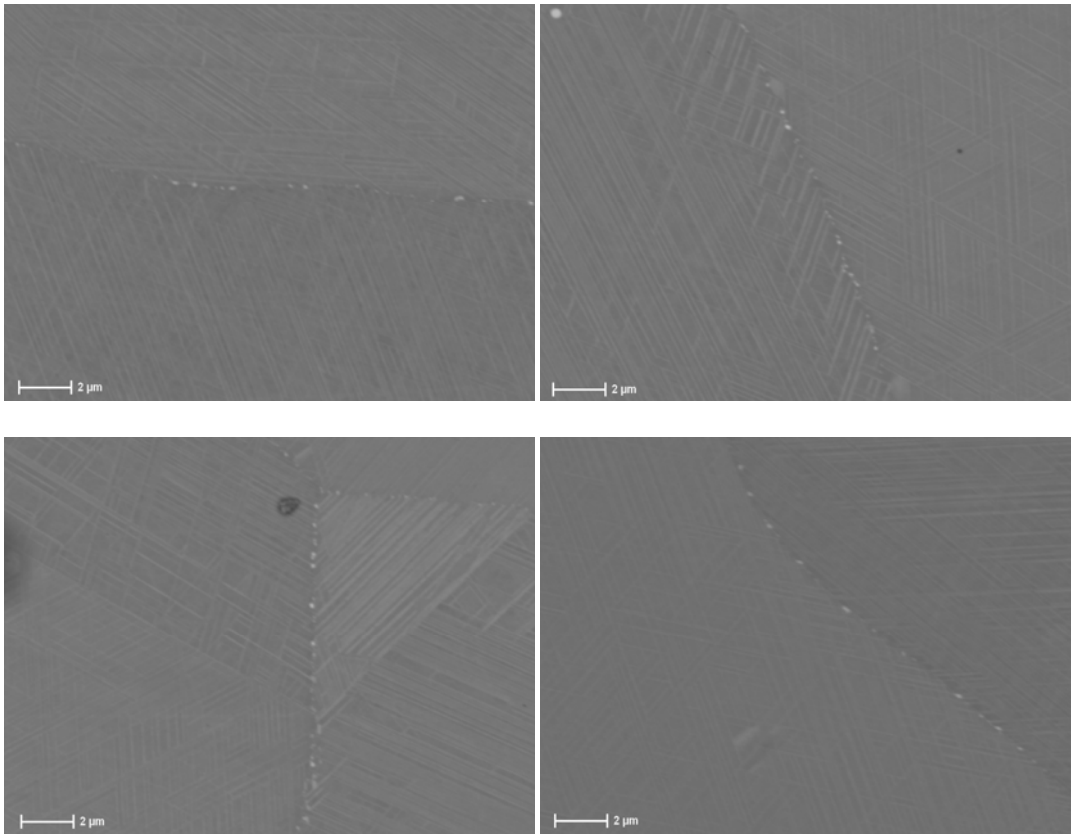

Image	Coverage	Average Size (µm^2)
64677	0.1621	0.1936
64678	0.2257	0.1286
64679	0.1513	0.1221
64680	0.1066	0.1446
Average	**0.1614**	**0.1472**
Standard Deviation	**0.0905**	**0.1256**
Standard Error	**0.0453**	**0.0628**

Aged 12000h at 675°C

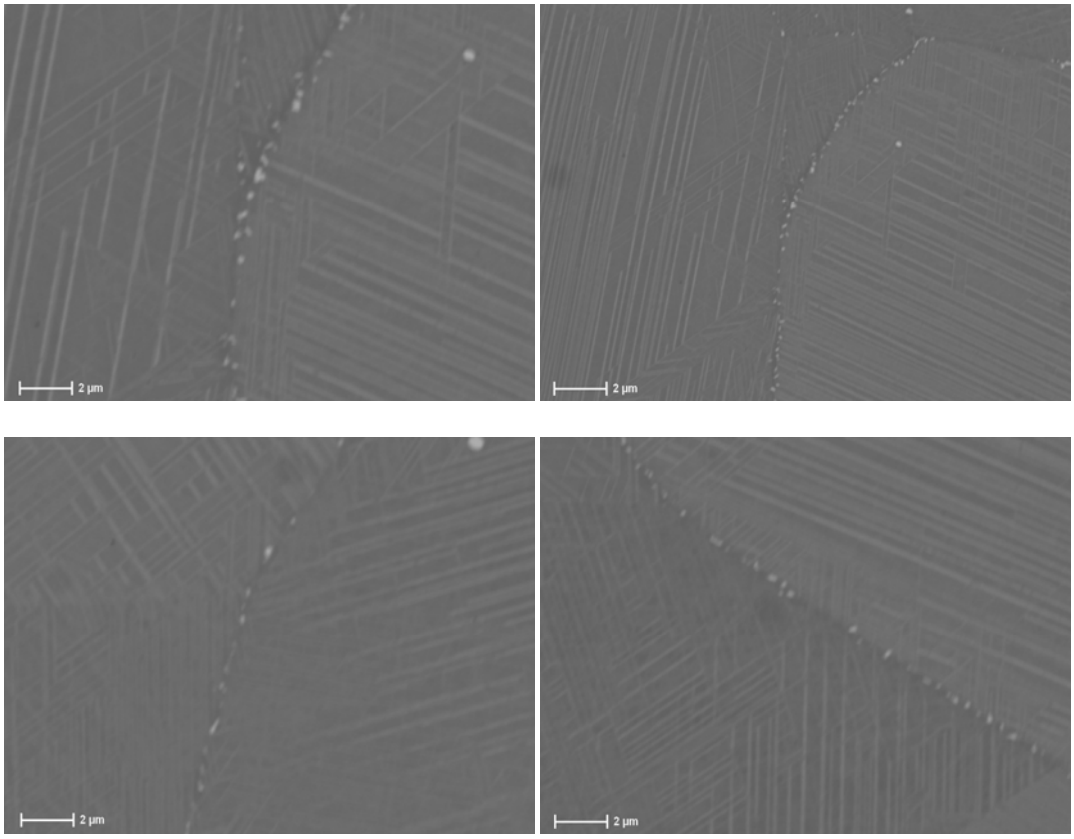

Image	Coverage	Average Size (µm^2)
64672	0.2978	0.4085
64674	0.1895	0.1541
64675	0.3038	0.3468
64676	0.2166	0.1819
Average	**0.2519**	**0.2728**
Standard Deviation	**0.0489**	**0.1048**
Standard Error	**0.0244**	**0.0524**

Aged 0.33h at 850°C

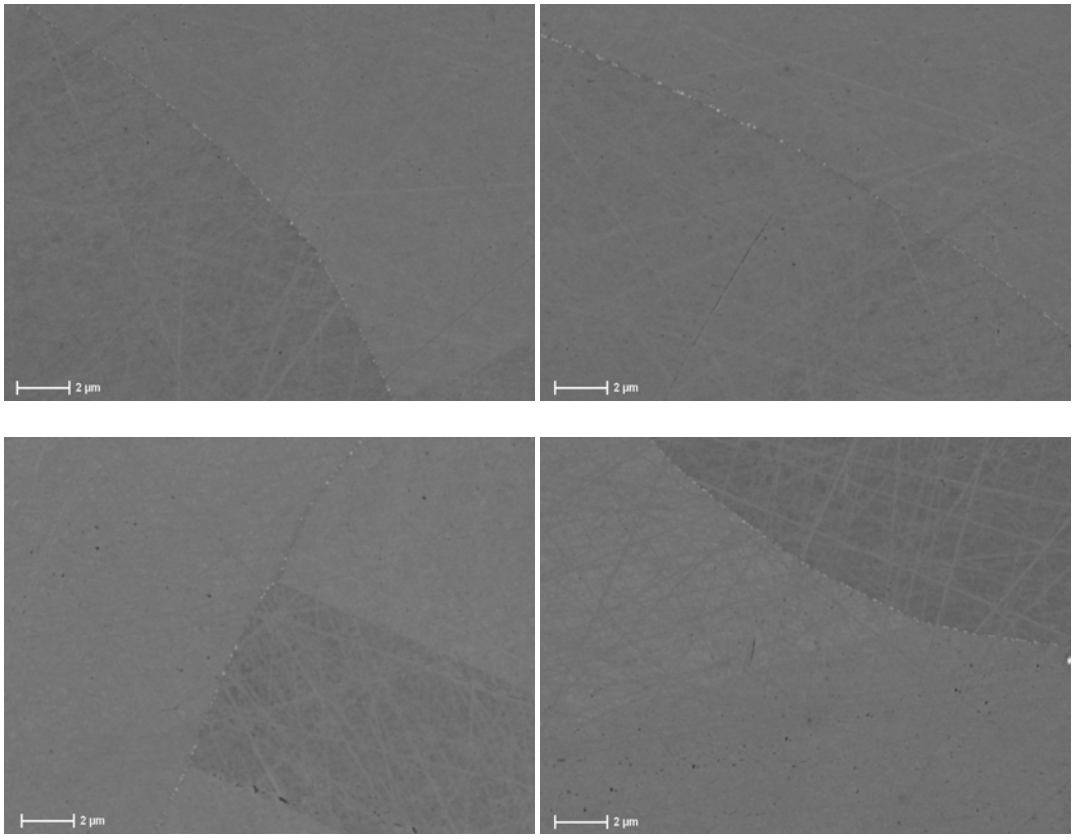

Image	Coverage	Average Size (um^2)
64687	0.0994	0.1077
64688	0.1299	0.0904
64689	0.1899	0.0771
64690	0.1668	0.0880
Average	**0.1465**	**0.0908**
Standard Deviation	**0.4078**	**1.2120**
Standard Error	**0.2039**	**0.6060**

Aged 9.5h at 850°C

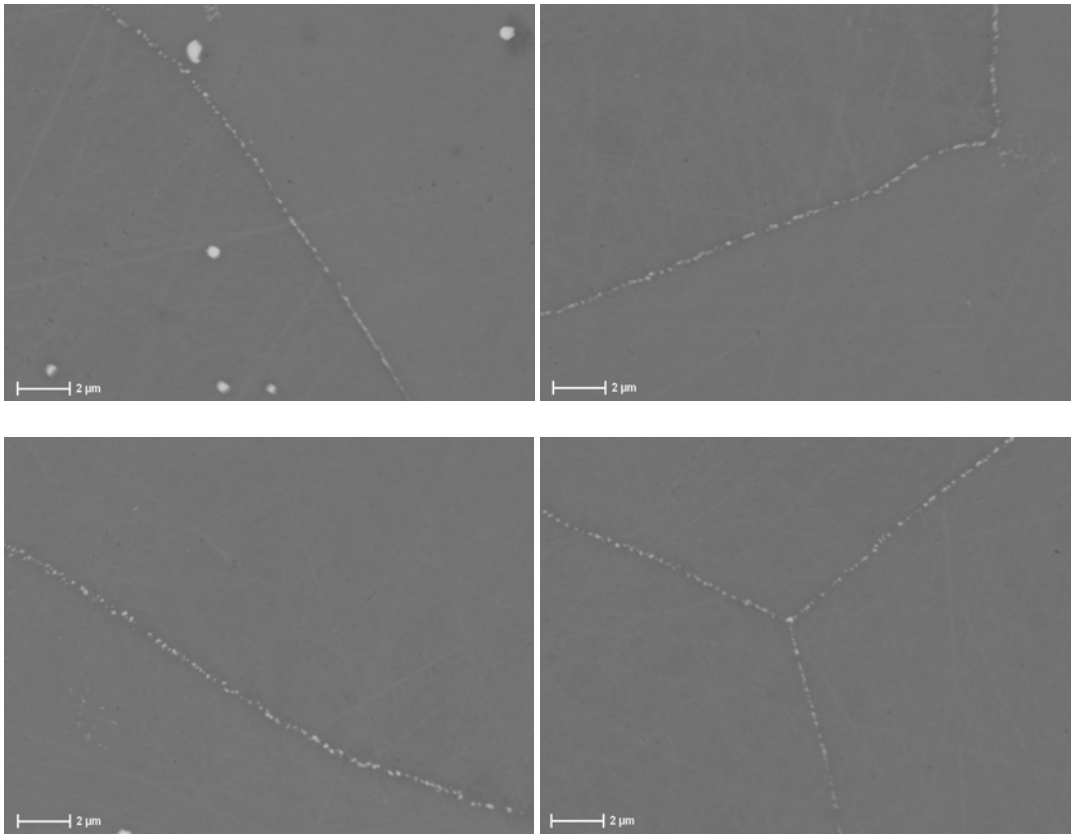

Image	Coverage	Average Size (um^2)
64909	0.3437	0.1249
64910	0.2987	0.1154
64912	0.1391	0.1152
64913	0.2697	0.1234
Average	**0.2628**	**0.1197**
Standard Deviation	**0.2915**	**1.1830**
Standard Error	**0.1457**	**0.5915**

Aged 57.6h at 850°C

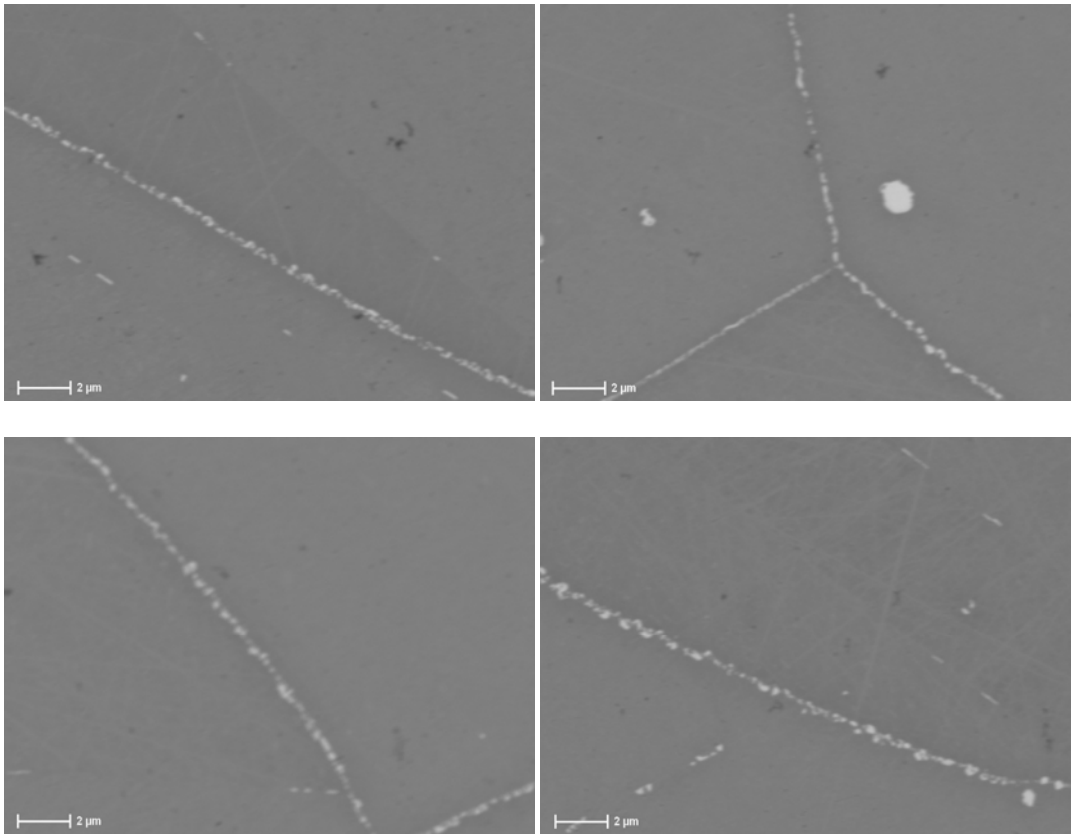

Image	Coverage	Average Size (um^2)
64681	0.3491	0.3100
64683	0.5219	0.2860
64684	0.4230	0.2501
64685	0.4258	0.2569
Average	**0.4300**	**0.2757**
Standard Deviation	**0.1243**	**1.0270**
Standard Error	**0.0622**	**0.5135**

Aged 2015h at 850°C

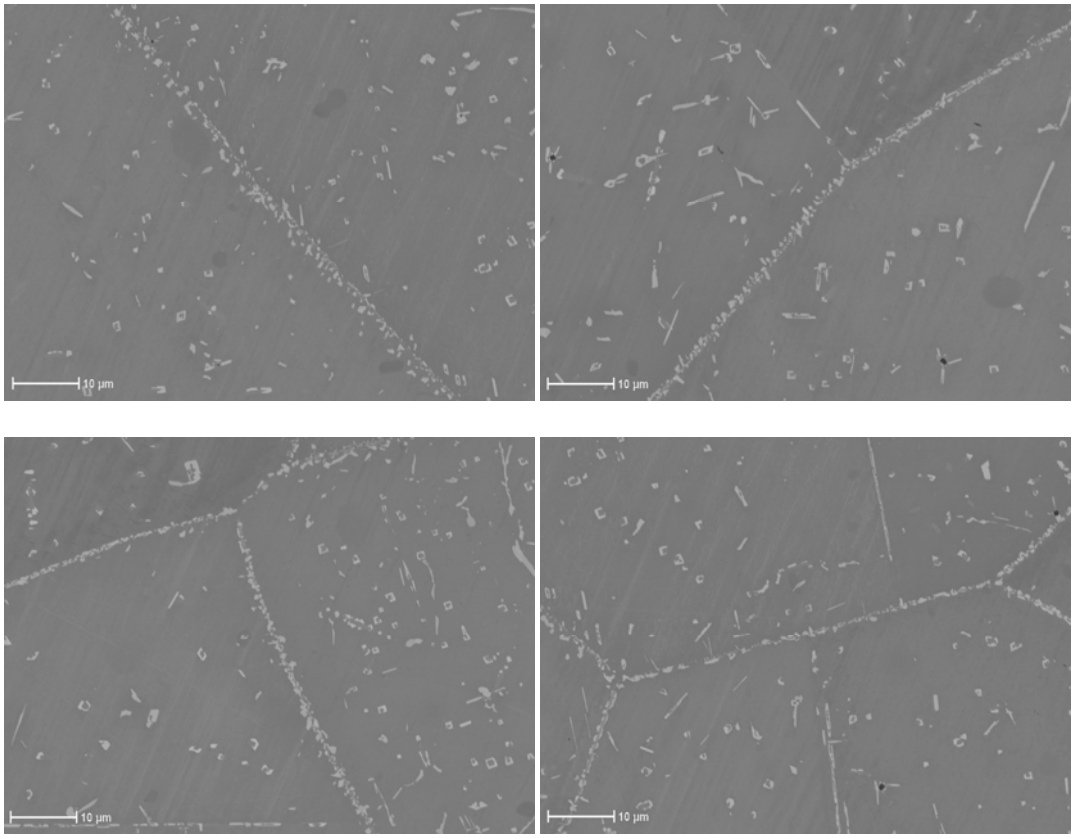

Image	Coverage	Average Size (um^2)
65228	0.4762	0.7756
65229	0.4443	0.6343
65230	0.3743	0.6186
65231	0.4680	0.8189
Average	**0.4407**	**0.7118**
Standard Deviation	**0.1136**	**0.5910**
Standard Error	**0.0568**	**0.2955**

Aged 8975h at 850°C

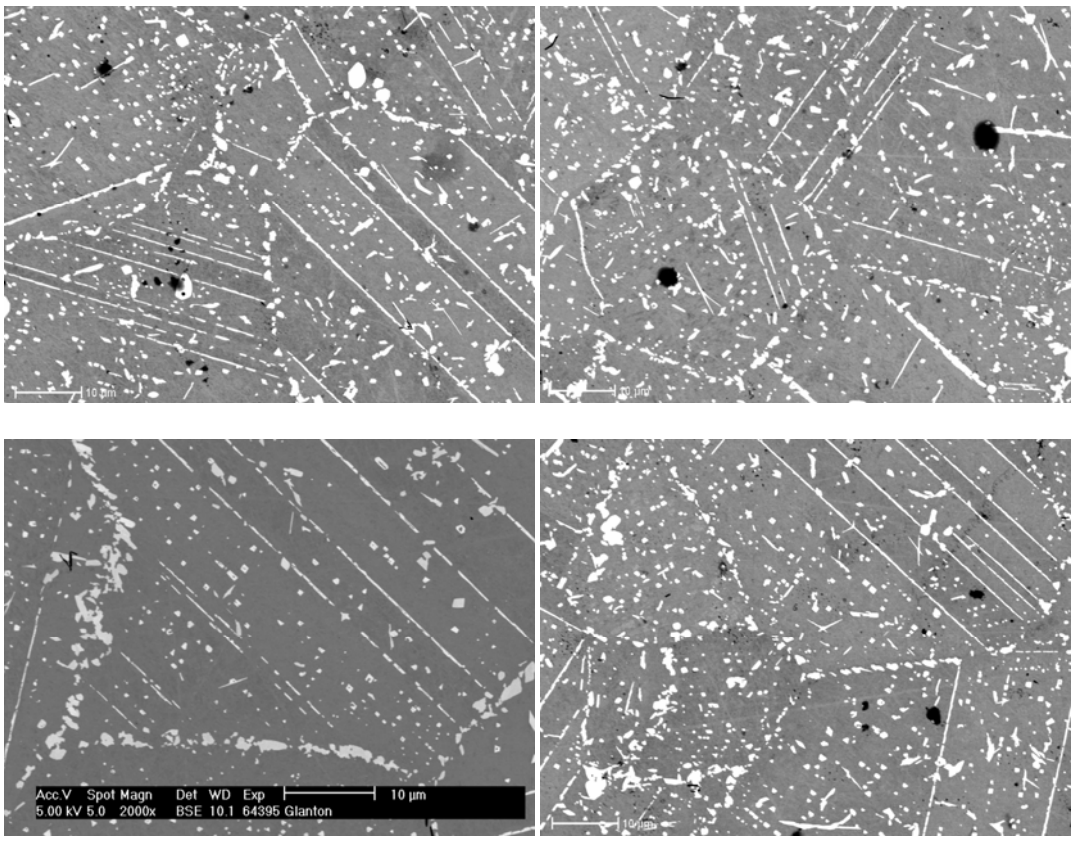

Image	Coverage	Average Size (um^2)
64395	0.6468	1.3187
64528	0.5769	1.5161
64529	0.5549	1.3548
64530	0.4385	1.0215
Average	**0.5543**	**1.3028**
Standard Deviation	**0.0579**	**0.1406**
Standard Error	**0.0289**	**0.0703**

Appendix B

Aged 6000h at 675°C

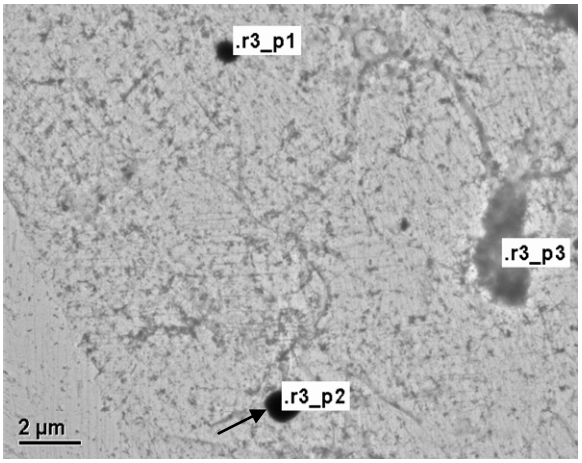

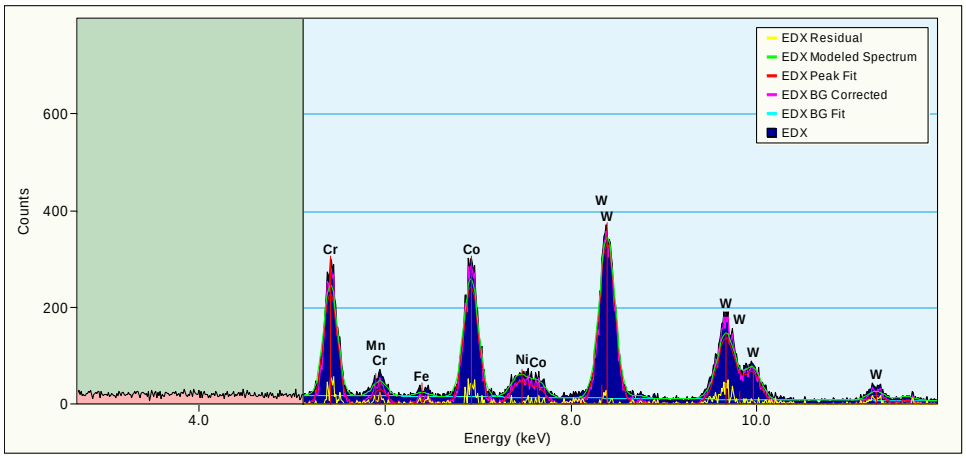

Element	Weight %	Atomic %	Uncertainty %	Correction	k-Factor
-------	--------	--------	----------	----------	--------
Cr(K)	10.713	22.921	0.154	0.991	1.376
Fe(K)	0.42	0.838	0.036	0.994	1.48
Co(K)	13.856	26.155	0.19	0.995	1.576
Ni(K)	2.177	4.126	0.102	0.996	1.592
Mo(K)	3.409	3.953	0.154	0.998	4.581
W(L)	69.422	42.005	0.622	0.752	5.419

Aged 6000h at 675°C

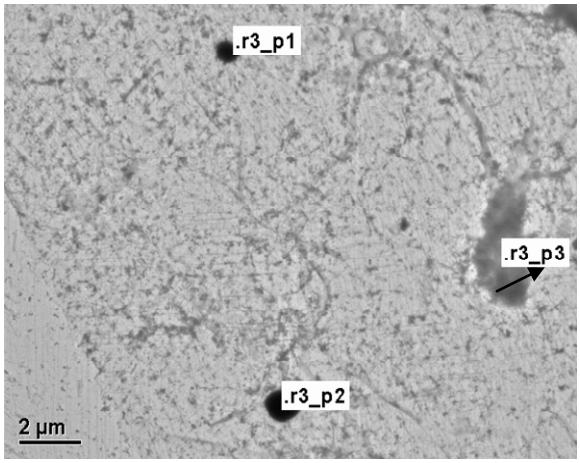

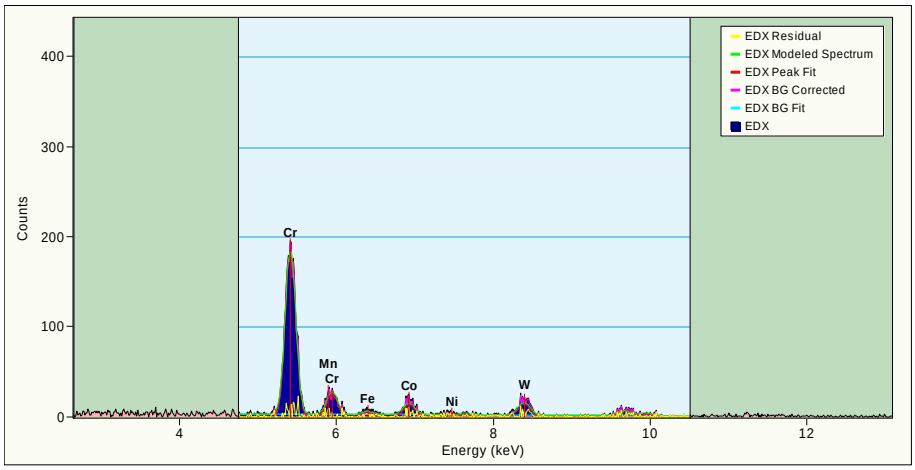

nent	Weight %	Atomic %	Uncertainty %	Correction	k-Factor
--	--------	--------	----------	----------	--------
;)	89.953	90.941	1.605	0.991	1.376
K)	0.089	0.085	0.532	0.993	1.451
;)	1.825	1.718	0.279	0.994	1.48
;)	7.636	6.811	0.514	0.995	1.576
;)	0.494	0.442	0.237	0.996	1.592
K)	0	0	100	0.998	4.581
;)	0	0	100	0.754	64.957

Aged 57.6h at 850°C

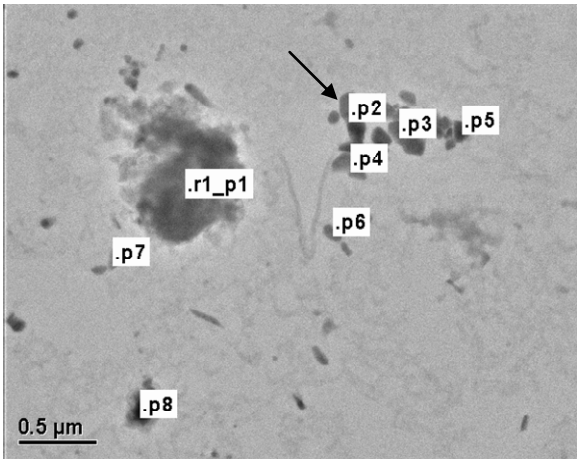

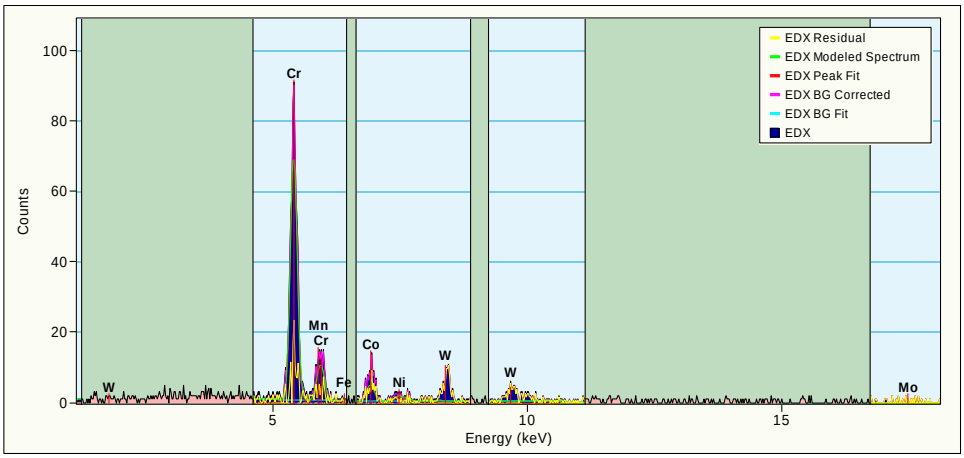

Element	Weight %	Atomic %	Uncertainty %	Correction	k-Factor
-------	--------	--------	----------	----------	--------
Cr(K)	88.793	89.869	2.661	0.991	1.376
Mn(K)	1.698	1.627	1.018	0.993	1.451
Fe(K)	0.097	0.091	0.433	0.994	1.48
Co(K)	7.113	6.352	0.832	0.995	1.576
Ni(K)	2.297	2.059	0.548	0.996	1.592
Mo(K)	0	0	100	0.998	4.581
W(K)	0	0	100	0.754	64.957

Aged 57.6h at 850°C

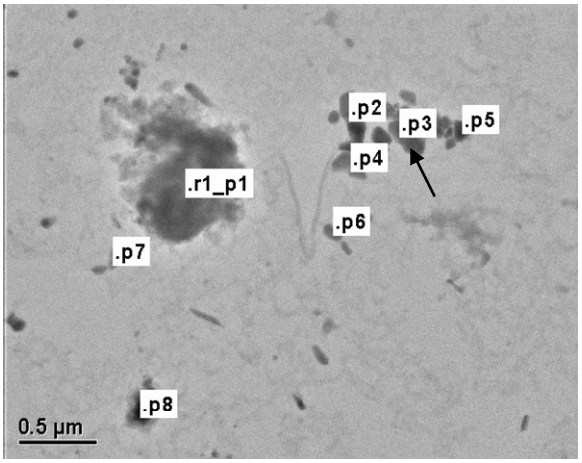

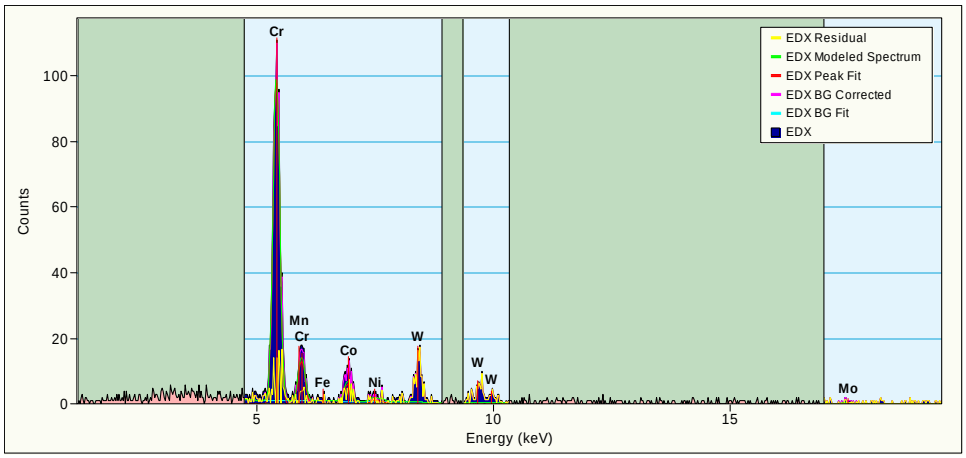

Element	Weight %	Atomic %	Uncertainty%	Correction	k-Factor
-------	--------	--------	----------	----------	--------
Cr(K)	88.988	91.01	2.096	0.991	1.376
Mn(K)	0	0	100	0.993	1.451
Fe(K)	0	0	100	0.994	1.48
Co(K)	6.831	6.164	0.675	0.995	1.576
Ni(K)	1.446	1.31	0.384	0.996	1.592
Mo(K)	2.733	1.515	1.153	0.998	4.581
W(K)	0	0	100	0.754	64.957

Aged 57.6h at 850°C

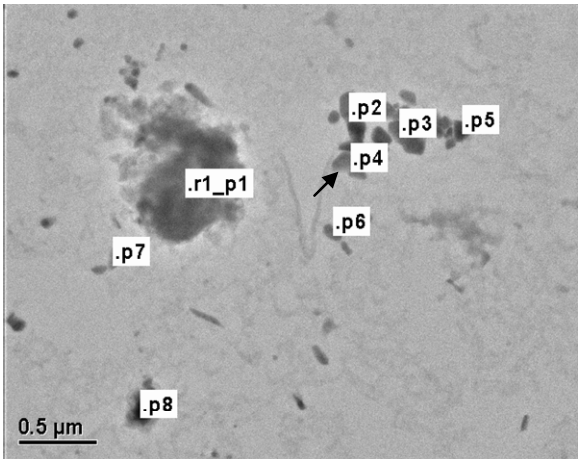

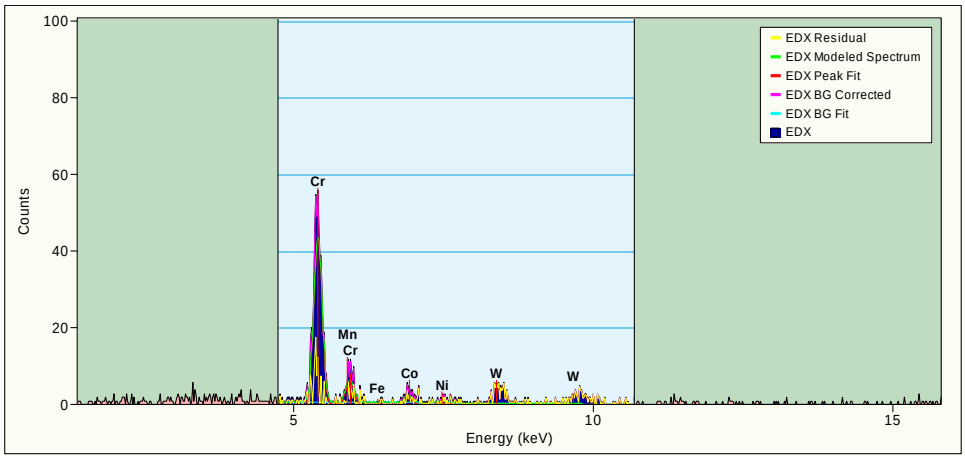

Element	Weight %	Atomic %	Uncertainty %	Correction	k-Factor
---	---	---	---	---	---
Cr(K)	93.516	94.23	3.463	0.991	1.376
Mn(K)	0	0	100	0.993	1.451
Fe(K)	0	0	100	0.994	1.48
Co(K)	4.923	4.377	0.993	0.995	1.576
Ni(K)	1.559	1.392	0.839	0.996	1.592
Mo(K)	0	0	100	0.998	4.581
W(K)	0	0	100	0.754	64.957

Aged 57.6h at 850°C

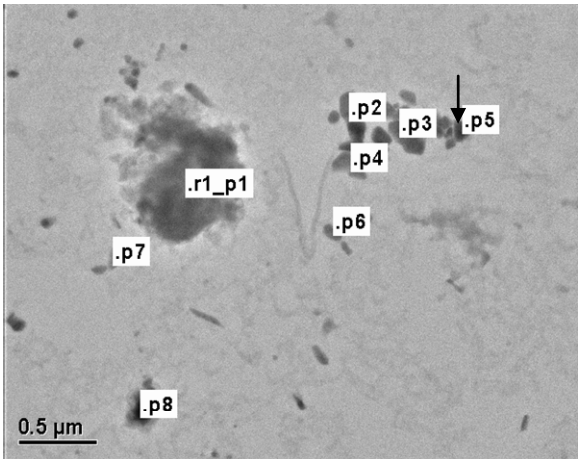

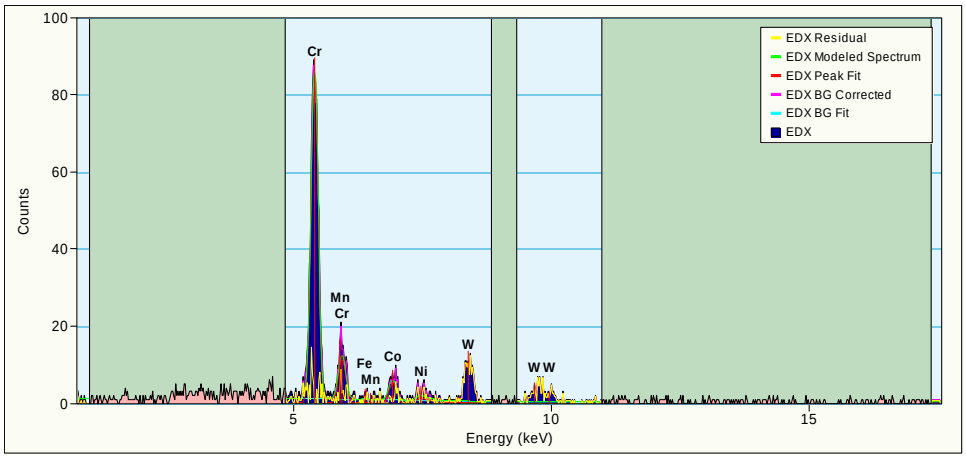

Element	Weight %	Atomic %	Uncertainty %	Correction	k-Factor
-------	--------	--------	----------	----------	--------
Cr(K)	88.984	90.907	2.264	0.991	1.376
Mn(K)	0	0	100	0.993	1.451
Fe(K)	0.229	0.218	0.351	0.994	1.48
Co(K)	6.537	5.892	0.696	0.995	1.576
Ni(K)	1.791	1.621	0.464	0.996	1.592
Mo(K)	2.456	1.36	1.301	0.998	4.581
W(K)	0	0	100	0.754	64.957

Aged 57.6h at 850°C

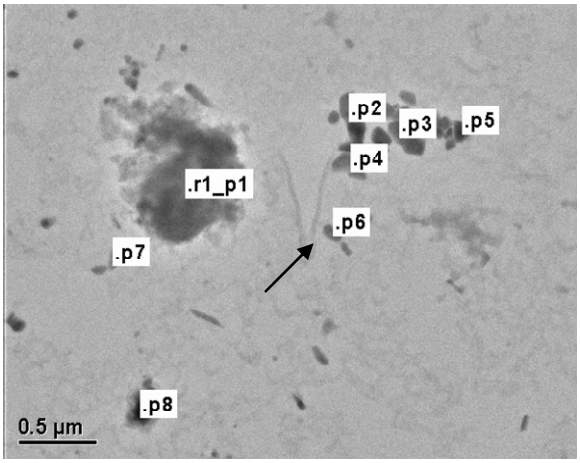

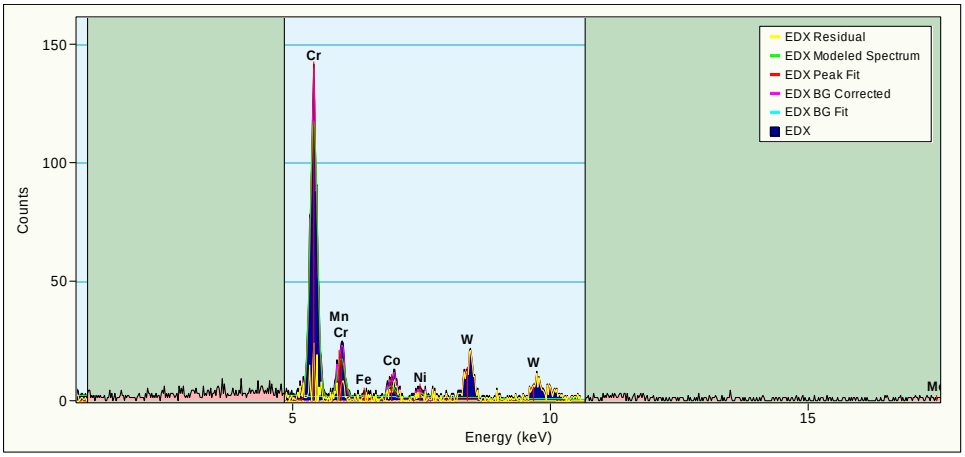

Element	Weight %	Atomic %	Uncertainty %	Correction	k-Factor
---	---	---	---	---	---
Cr(K)	92.575	93.443	2.157	0.991	1.376
Mn(K)	0.453	0.433	0.759	0.993	1.451
Fe(K)	0.353	0.332	0.298	0.994	1.48
Co(K)	4.62	4.114	0.53	0.995	1.576
Ni(K)	1.68	1.502	0.369	0.996	1.592
Mo(K)	0.316	0.173	1.005	0.998	4.581
W(K)	0	0	100	0.754	64.957

Aged 57.6h at 850°C

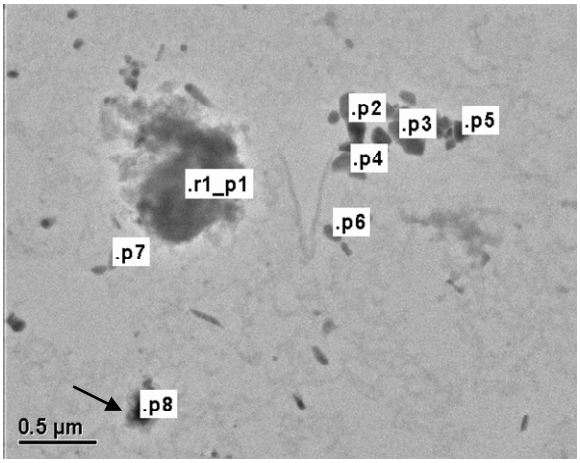

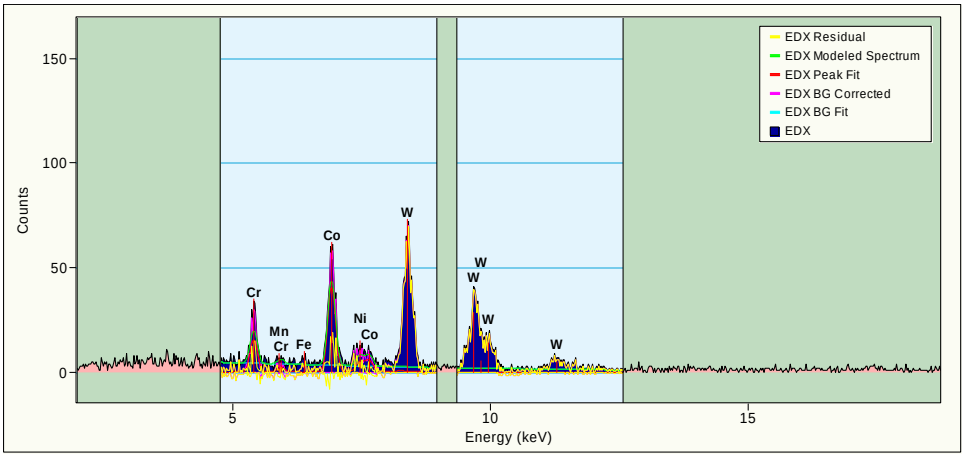

Element	Weight %	Atomic %	Uncertainty %	Correction	k-Factor
-------	--------	--------	-----------	----------	--------
Cr(K)	20.278	22.86	1.278	0.991	1.376
Mn(K)	0	0	100	0.993	1.451
Fe(K)	0	0	100	0.994	1.48
Co(K)	65.74	65.386	2.39	0.995	1.576
Ni(K)	8.285	8.273	0.968	0.996	1.592
Mo(K)	5.696	3.48	1.828	0.998	4.581
W(K)	0	0	100	0.754	64.957

Aged 8975h at 850°

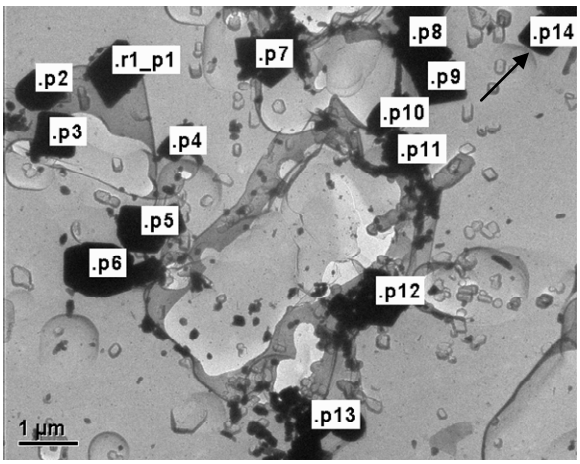

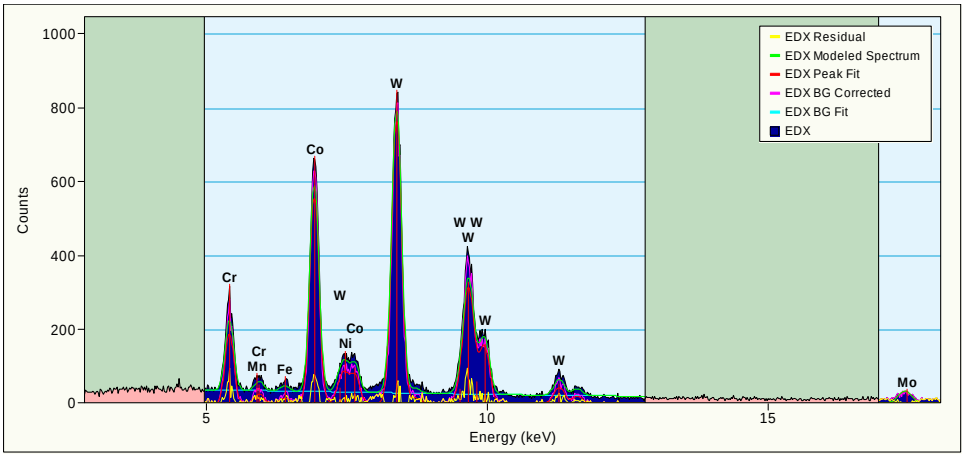

Element	Weight %	Atomic %	Uncertainty %	Correction	k-Factor
-------	--------	--------	----------	----------	--------
Cr(K)	4.143	9.764	0.066	0.991	1.376
Fe(K)	0.337	0.741	0.022	0.994	1.48
Co(K)	14.935	31.049	0.135	0.995	1.576
Ni(K)	1.723	3.597	0.065	0.996	1.592
Mo(K)	3.756	4.797	0.11	0.998	4.581
W(L)	75.102	50.049	0.443	0.752	5.419

Aged 8975h at 850°

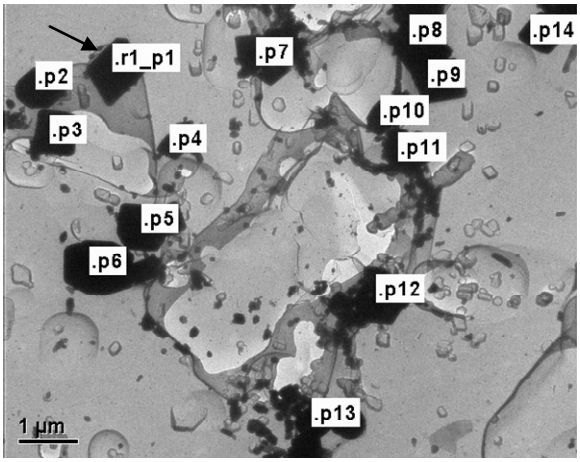

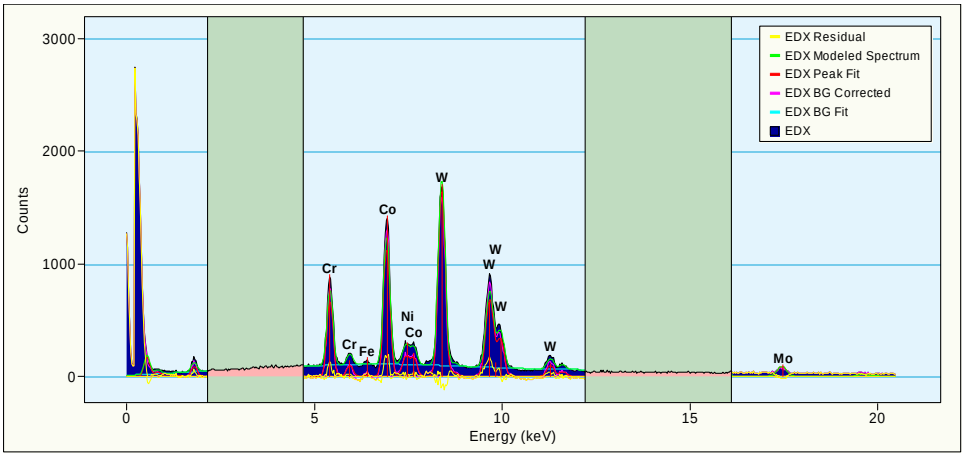

Element	Weight %	Atomic %	Uncertainty %	Correction	k-Factor
-------	--------	--------	----------	----------	--------
Cr(K)	6.659	15.343	0.056	0.991	1.376
Fe(K)	0.046	0.1	0.008	0.994	1.48
Co(K)	13.728	27.908	0.087	0.995	1.576
Ni(K)	1.576	3.217	0.042	0.996	1.592
Mo(K)	4.362	5.447	0.08	0.998	4.581
W(L)	73.627	47.981	0.296	0.752	5.419

Aged 8975h at 850°

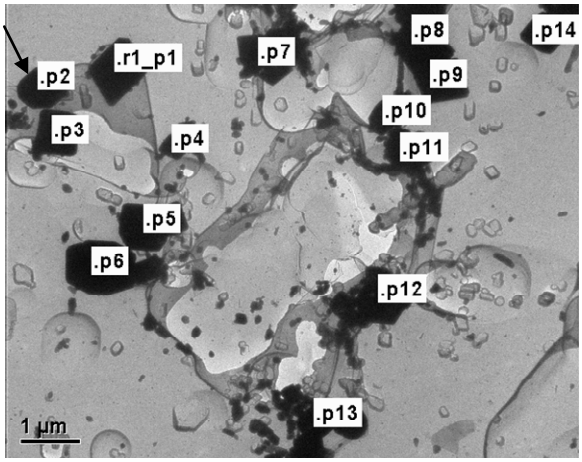

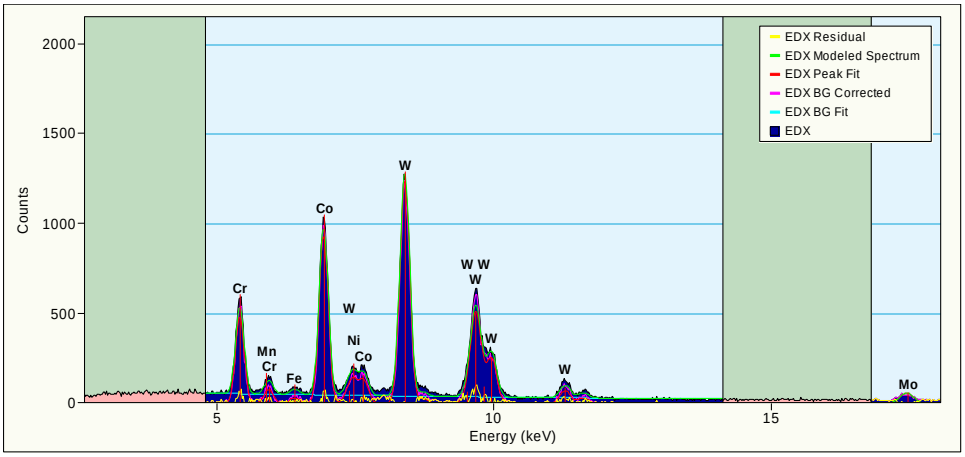

Element	Weight %	Atomic %	Uncertainty %	Correction	k-Factor
-------	--------	--------	----------	----------	--------
Cr(K)	6.314	14.312	0.065	0.991	1.376
Mn(K)	0.185	0.398	0.026	0.993	1.451
Fe(K)	0.406	0.858	0.018	0.994	1.48
Co(K)	14.795	29.585	0.104	0.995	1.576
Ni(K)	1.698	3.409	0.05	0.996	1.592
Mo(K)	3.977	4.885	0.088	0.998	4.581
W(L)	72.622	46.55	0.336	0.752	5.419

Aged 8975h at 850°

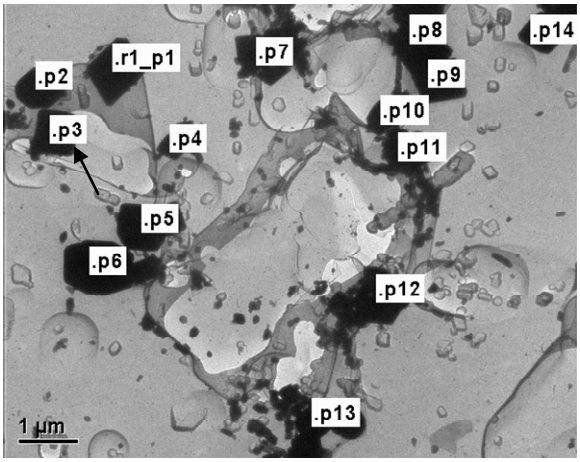

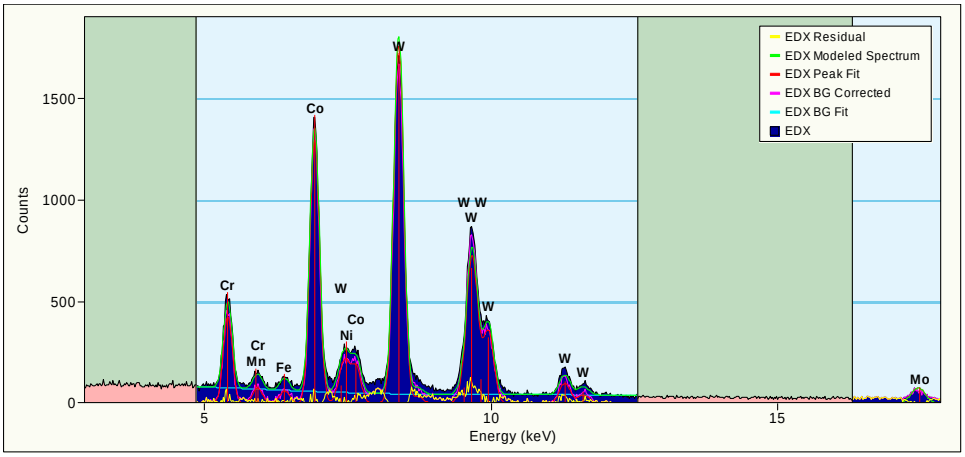

Element	Weight %	Atomic %	Uncertainty%	Correction	k-Factor
-------	--------	--------	----------	----------	--------
Cr(K)	4.054	9.466	0.044	0.991	1.376
Mn(K)	0.201	0.445	0.019	0.993	1.451
Fe(K)	0.63	1.37	0.018	0.994	1.48
Co(K)	14.982	30.865	0.089	0.995	1.576
Ni(K)	1.918	3.968	0.044	0.996	1.592
Mo(K)	3.694	4.674	0.072	0.998	4.581
W(L)	74.518	49.209	0.289	0.752	5.419

Aged 8975h at 850°

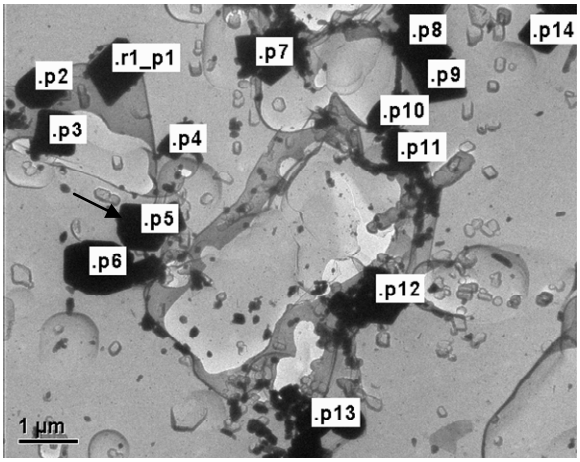

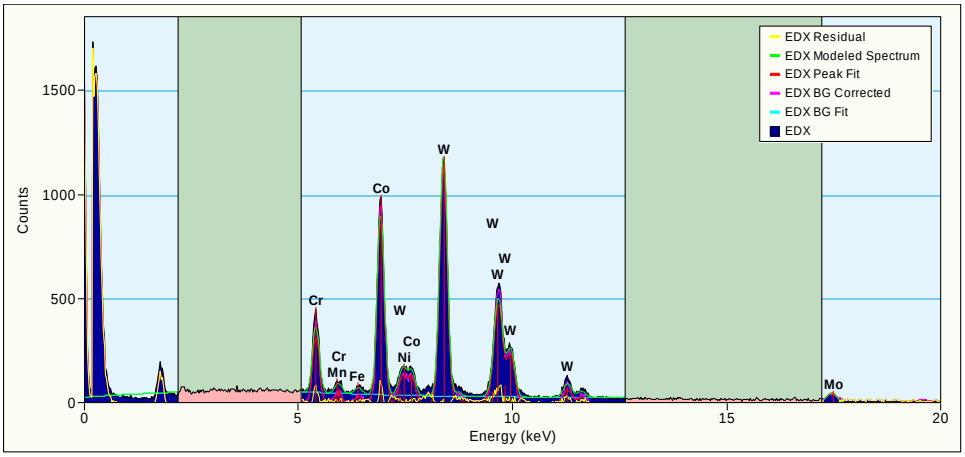

Element	Weight %	Atomic %	Uncertainty %	Correction	k-Factor
-------	--------	--------	----------	----------	--------
Cr(K)	4.558	10.59	0.059	0.991	1.376
Mn(K)	0.096	0.212	0.023	0.993	1.451
Fe(K)	0.473	1.023	0.02	0.994	1.48
Co(K)	15.177	31.108	0.11	0.995	1.576
Ni(K)	1.762	3.627	0.053	0.996	1.592
Mo(K)	3.713	4.675	0.089	0.998	4.581
W(L)	74.217	48.761	0.357	0.752	5.419

Aged 8975h at 850°

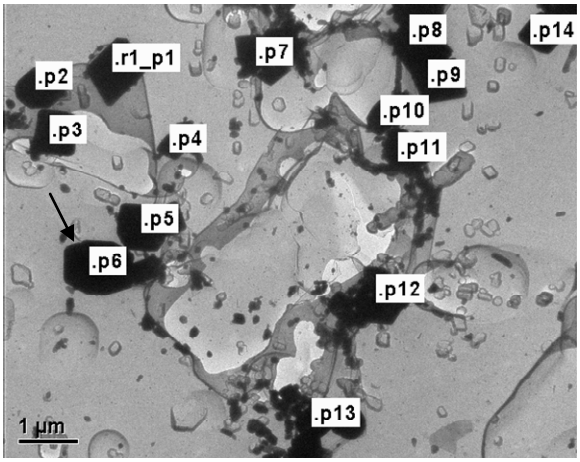

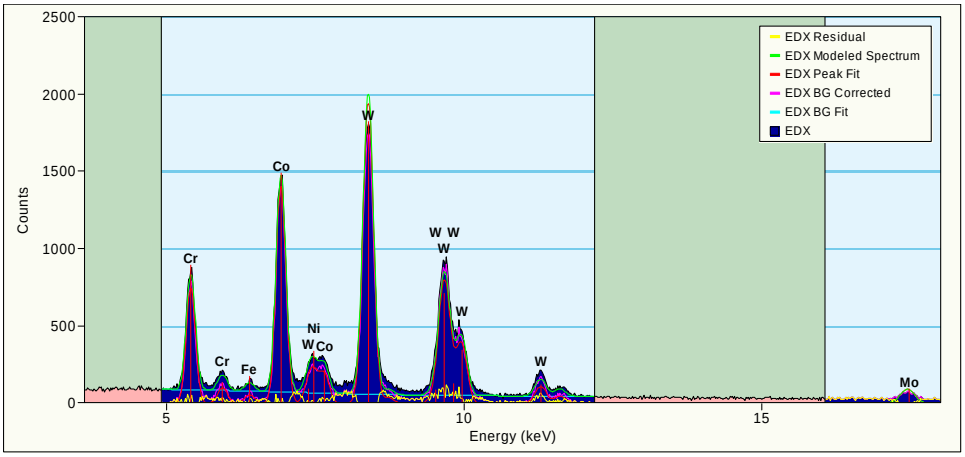

Element	Weight %	Atomic %	Uncertainty %	Correction	k-Factor
-------	--------	--------	----------	----------	--------
Cr(K)	6.289	14.338	0.05	0.991	1.376
Fe(K)	0.501	1.063	0.015	0.994	1.48
Co(K)	14.419	29	0.082	0.995	1.576
Ni(K)	1.817	3.67	0.04	0.996	1.592
Mo(K)	3.898	4.816	0.069	0.998	4.581
W(L)	73.074	47.111	0.27	0.752	5.419

Aged 8975h at 850°

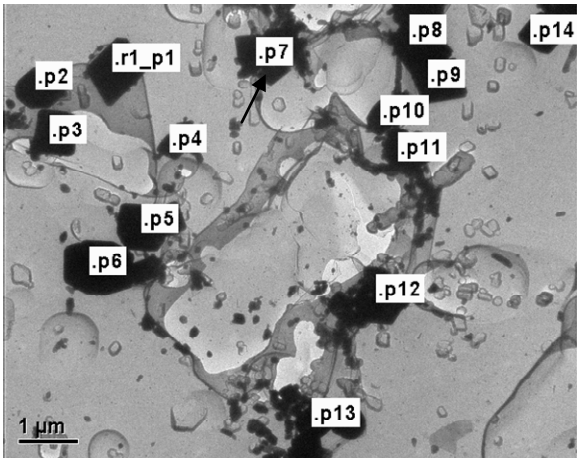

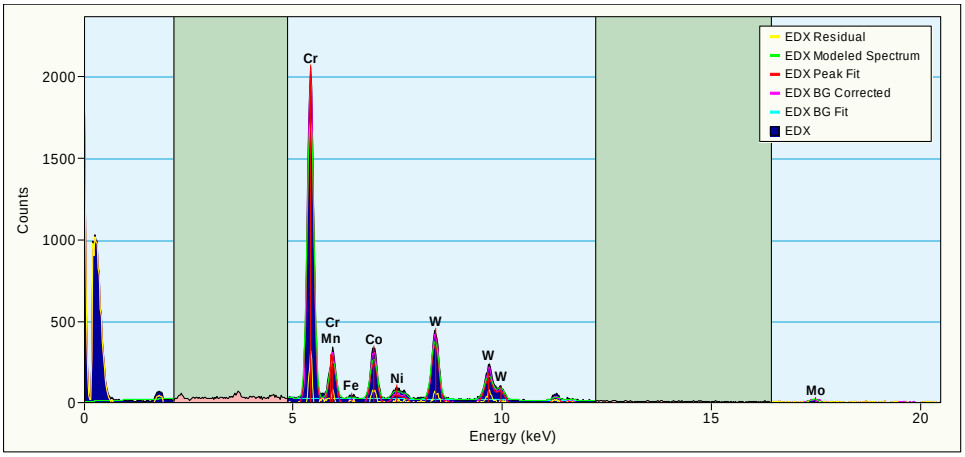

Element	Weight %	Atomic %	Uncertainty %	Correction	k-Factor
-------	--------	--------	----------	----------	--------
Cr(K)	45.791	67.906	0.24	0.991	1.376
Fe(K)	0.184	0.254	0.021	0.994	1.48
Co(K)	7.879	10.309	0.109	0.995	1.576
Ni(K)	1.19	1.563	0.059	0.996	1.592
Mo(K)	2.893	2.325	0.107	0.998	4.581
W(L)	42.061	17.64	0.371	0.752	5.419

Aged 8975h at 850°

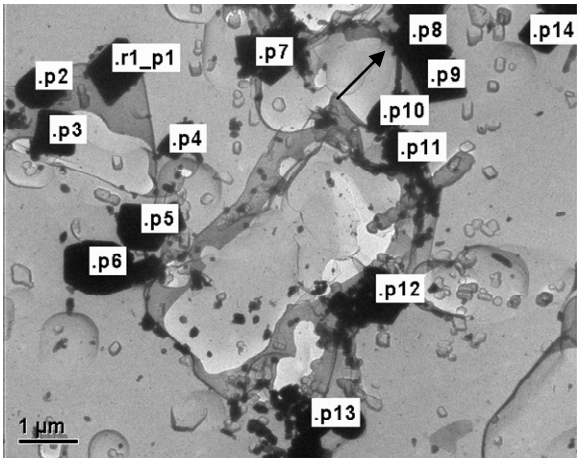

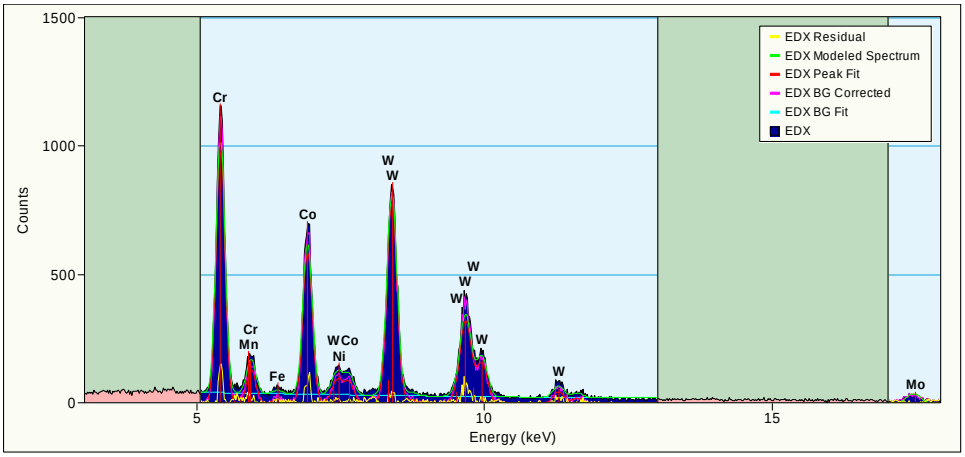

Element	Weight %	Atomic %	Uncertainty %	Correction	k-Factor
-------	--------	--------	----------	----------	--------
Cr(K)	17.956	35.178	0.124	0.991	1.376
Fe(K)	0.278	0.508	0.019	0.994	1.48
Co(K)	13.052	22.56	0.115	0.995	1.576
Ni(K)	1.61	2.795	0.057	0.996	1.592
Mo(K)	3.502	3.719	0.097	0.998	4.581
W(L)	63.599	35.238	0.372	0.752	5.419

Aged 8975h at 850°

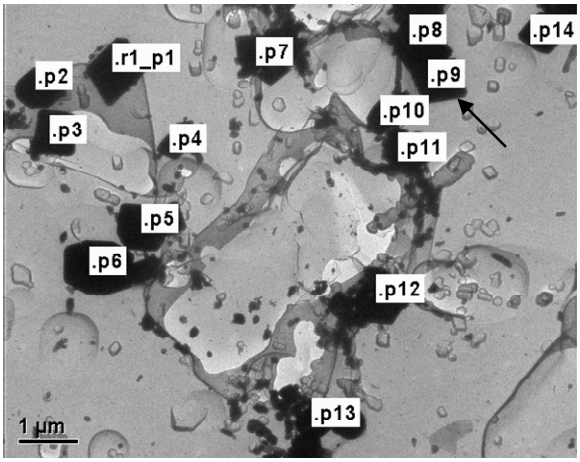

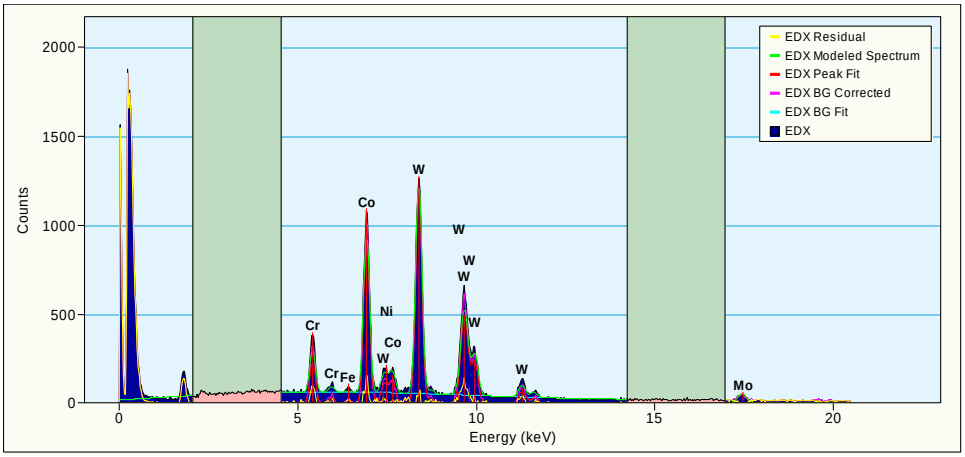

Element	Weight %	Atomic %	Uncertainty %	Correction	k-Factor
-------	--------	--------	----------	----------	--------
Cr(K)	3.359	8.026	0.049	0.991	1.376
Fe(K)	0.08	0.178	0.012	0.994	1.48
Co(K)	15.398	32.458	0.112	0.995	1.576
Ni(K)	1.426	3.019	0.051	0.996	1.592
Mo(K)	3.939	5.101	0.092	0.998	4.581
W(L)	75.796	51.216	0.364	0.752	5.419

Aged 8975h at 850°

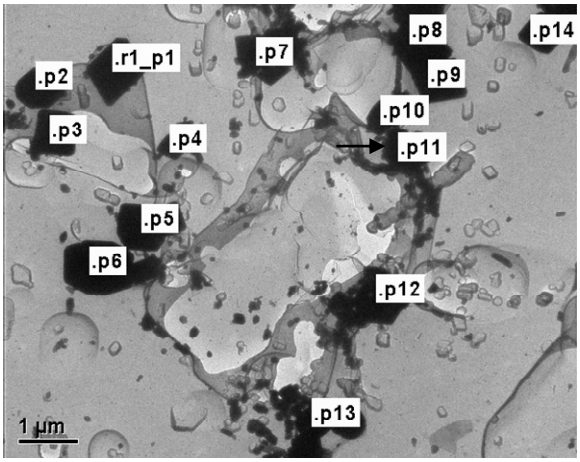

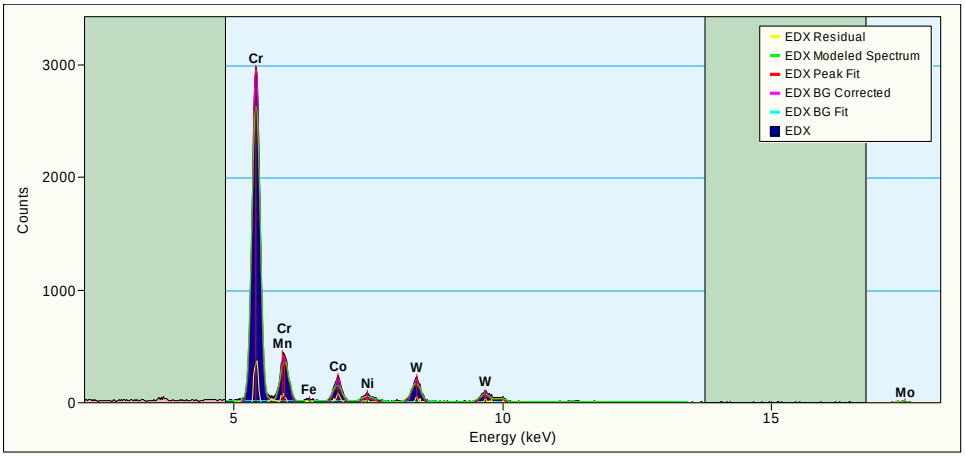

Element	Weight %	Atomic %	Uncertainty %	Correction	k-Factor
-------	--------	--------	----------	----------	--------
Cr(K)	72.233	85.636	0.307	0.991	1.376
Fe(K)	0.157	0.174	0.02	0.994	1.48
Co(K)	4.636	4.849	0.086	0.995	1.576
Ni(K)	1.365	1.433	0.058	0.996	1.592
Mo(K)	2.152	1.383	0.093	0.998	4.581
W(L)	19.454	6.523	0.259	0.752	5.419

Aged 8975h at 850°

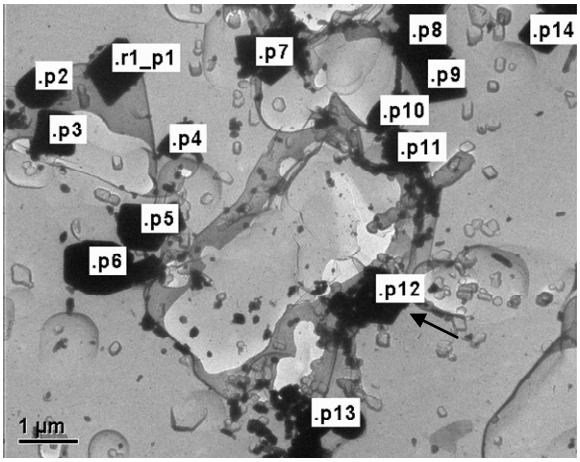

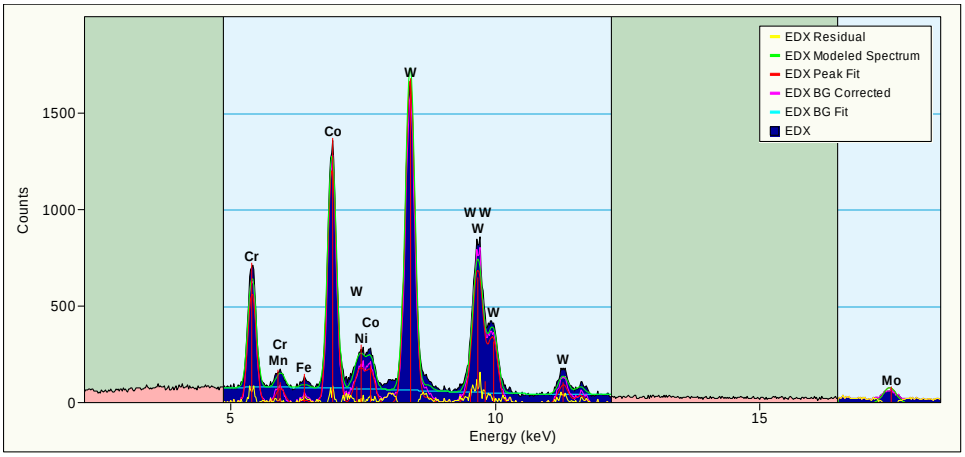

Element	Weight %	Atomic %	Uncertainty %	Correction	k-Factor
-------	--------	--------	----------	----------	--------
Cr(K)	5.606	12.99	0.051	0.991	1.376
Fe(K)	0.175	0.378	0.011	0.994	1.48
Co(K)	14.515	29.673	0.089	0.995	1.576
Ni(K)	1.599	3.283	0.042	0.996	1.592
Mo(K)	4.151	5.213	0.078	0.998	4.581
W(L)	73.951	48.46	0.294	0.752	5.419

Aged 8975h at 850°

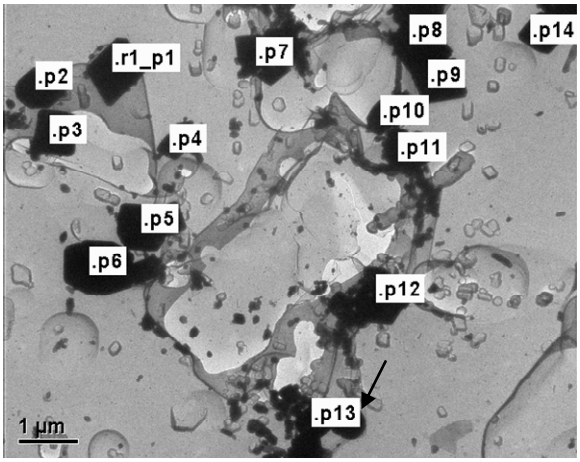

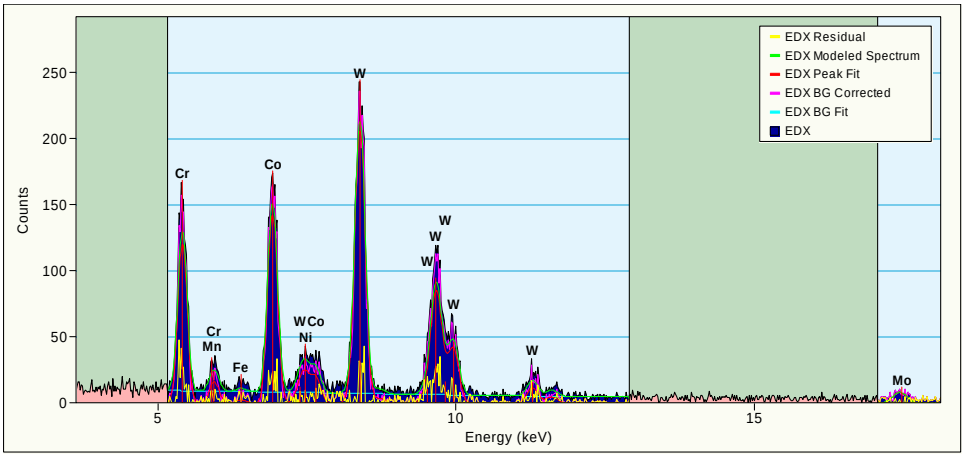

Element	Weight %	Atomic %	Uncertainty %	Correction	k-Factor
-------	--------	--------	----------	----------	--------
Cr(K)	9.417	20.812	0.187	0.991	1.376
Fe(K)	0.212	0.437	0.04	0.994	1.48
Co(K)	13.555	26.43	0.243	0.995	1.576
Ni(K)	1.822	3.567	0.125	0.996	1.592
Mo(K)	3.285	3.935	0.196	0.998	4.581
W(L)	71.705	44.816	0.821	0.752	5.419

Vita

Darryl Britt Glanton was born in Tuscaloosa, AL on April 18, 1982. He was raised in Dothan, AL and attended high school at The Alabama School of Mathematics and Science. He graduated in 2000. From there he went to North Carolina State University as a Park Scholar. He received a B.S. in Materials Science and Engineering in 2005.

Darryl is currently participating in the Post-Bachelor's research program at Oak Ridge National Laboratory and is concurrently pursuing his Master of Science in Materials Science and Engineering at the University of Tennessee, Knoxville.